Apollo Next Generation Sample Analysis (ANGSA) samples: Preliminary Examination of Double Drive Tube Samples 73001 and 73002 and Lessons Learned for Returning to the Moon with Artemis.

[1,2,3]Juliane Gross, [1]Ryan A. Zeigler, [4]Andrea B. Mosie, [4]Charis Krysher, [4]Scott A. Eckley, [5]Richard A. Ketcham, [5]Romy D. Hanna, [5]David Edey, [4]Jeremy J. Kent, [1]Francis M. McCubbin, [6]Francesca McDonald, [6,7]Timon Schild, [8]Paul G. Lucey, [8]Lingzhi Sun, [8]Abigail Flom, [9]Rita Parai, [10]Alex Meshik, [10]Olga Pravdivtseva, [11]Noah E. Petro, [12,2]Charles K. Shearer, and the [13]ANGSA Science Team.

[1]Astromaterials Acquisition and Curation Office, NASA Johnson Space Center, Houston, TX, USA

[2]Lunar and Planetary Institute, Houston TX, USA

[3]The American Museum of Natural History, Dept. Earth and Planetary Sciences; New York, NY, USA

[4]GeoControl Systems Inc., Jacobs JETS Contract, NASA Johnson Space Center, Houston, TX, USA

[5]Jackson School of Geosciences, University of Texas, Austin, TX, USA

[6]European Space Agency, ESTEC, Nordwijk, Netherlands

[7] now at European Space Resources Innovation Centre, ESRIC, Luxembourg,

[8]Department of Earth Sciences, Hawai‘i Institute of Geophysics and Planetology, University of Hawai‘i at Manoa, HI, USA

[9]Department of Earth, Environmental and Planetary Sciences, Washington University in St. Louis, St. Louis, MO 63130 USA

[10]Physics Department, Washington University, Saint Louis, MO 63130, USA.

[11]Solar System Exploration Division, NASA Goddard Space Flight Center, Greenbelt, Maryland, USA

[12]Dept. of Earth and Planetary Science, Institute of Meteoritics, University of New Mexico, Albuquerque, New Mexico 87131

[13]Apollo Next Generation Sample Analysis (ANGSA) Science Team, https://www.lpi.usra.edu/ANGSA/teams/

Key points:

1. Curation plays a crucial part in all stages of the Artemis missions to return samples, to ensure the integrity, and maximize their scientific return.
2. Preliminary examination of 73001/2 represents the first modern dissection of an Apollo core and helps us prepare for Artemis samples return.
3. Samples returned from the surface and subsurface of the Moon during upcoming Artemis missions are critical for informing future exploration.

Abstract:

During the six Apollo missions, astronauts collected 2196 lunar samples, nearly all of which have been studied over the past five decades. Six Apollo samples remained unexamined until 2019, saved to be analyzed by the next generation of lunar scientists using advanced modern laboratory facilities. Now more than 50 years after Apollo, NASA is returning to the Moon with Artemis and will return geologic samples from a different region of the lunar surface than Apollo. Curation will play an instrumental role in helping to prepare for the safe return of these valuable samples, ensuring their integrity during all stages of the missions, and thus maximizing their scientific return. To prepare for the return of these samples, NASA initiated the Apollo Next Generation Sample Analysis (ANGSA) Program to open previously unstudied samples including unopened double drive tube 73002 and 73001 (also vacuum-sealed) from the Apollo 17 mission to the Taurus-Littrow Valley. The ANGSA program was designed to function as a low-cost analog sample return mission and served as a testing ground to understand processes, update techniques, and prepare for the preliminary examination (PE) for the to-be-returned lunar samples with Artemis. New and advanced curation techniques were developed and applied to support the analyses of 73002/73001 during the PE. Furthermore, cutting-edge analytical instruments such as X-ray Computed Tomography were utilized to aid in PE that were unavailable during Apollo. These efforts are equipping the Artemis generation for future lunar missions and lessons learned from PE of ANGSA samples will be directly applied to Artemis.

Plain Language:

During the six Apollo missions, astronauts collected 2196 lunar samples, nearly all of which have been studied over the past 50 years. Six Apollo samples have been saved to be analyzed by the next generation of lunar scientists, using better and more advanced instruments. Now more than 50 years after Apollo, NASA is returning to the Moon with Artemis to bring back geologic samples from a different region of the Moon than Apollo. Curation will play an instrumental role in helping to prepare for the safe return of these valuable samples. To prepare for the return of these samples, NASA initiated the Apollo Next Generation Sample Analysis (ANGSA) Program to open the previously unstudied samples including double drive tube 73002 and 73001 from the Apollo 17 mission to the Taurus-Littrow Valley. The ANGSA program was designed as a low-cost analog sample return mission to test and update processes and techniques

for the preliminary examination (PE) in preparation of the soon-to-be returned samples with Artemis. These efforts and lessons learned are equipping the Artemis generation for future lunar missions and sample return from the Moon.

Keywords: Moon, Artemis, Apollo Next Generation Sample Analysis (ANGSA) initiative, curation, preliminary examination, X-ray computed tomography, gas extraction, dissection, Apollo 73002, Apollo 73001, drive tubes.

1. Introduction

The 382 kg of returned samples from the six Apollo missions provided for the first time the opportunity to study the Moon in detail with samples. From these samples we learned that the Moon serves as a museum of planetary history for the Earth and inner solar system, recording and preserving events that happened billions of years ago (e.g., Crawford et al., 2014, 2021). Most if not all the returned samples represent either samples of the primary crust, additions made to the crust, or modifications made to the crust (Figure 1) – the latter two are often referred to as “secondary crust” – and serve as the cornerstone of our understanding for lunar and planetary science (e.g., Gaddis et al., 2023; Elardo et al., 2023; Gaffney et al., 2023; Neal et al., 2023 and references therein). Apollo samples are used to further our understanding of lunar and solar system history and dynamics, including (Figure 2):

a) calibrating compositional information obtained by Earth-based telescopic observations (e.g., Charette et al., 1974) and space craft remote sensing instruments in orbit or when they fly past the Moon (e.g., Lucey et al., 1995, 1998, 2000a, 2006, 2017; Elphic et al., 1998, 2000, 2002; Feldman et al., 1998, 2000; Lawrence et al., 1998, 1999, 2000; Green et al., 2011; Grande et al., 2001; Prettyman et al., 2006; Athiray et al., 2013; Donnaldson-Hanna et al., 2017; Sato et al., 2017; Naito et al., 2018; Swinyard et al., 2009; Jones et al 2020; Sun et al., 2021a);

b) calibrating the lunar crater counting curve by providing absolute ages of sampled surface features (e.g., Hiesinger et al. 2000, 2003, 2010, 2011, 2012; 2023; Lucey et al. 2000b; Nyquist et al. 2001; Gaffney et al. 2008);

c) providing porosity and density data to understand global gravity datasets such as those produced by the Gravity Recovery and Interior Laboratory (GRAIL) mission (e.g., Wieczorek et al., 2013; Zuber et al., 2013; Kiefer et al. 2014);
d) revealing a variety of lunar evolutionary processes through sample petrology and geochemistry such as magma ocean evolution, volcanism, and core formation processes (e.g., Wood 1975; Simon et al., 1983, 1984; Hallis et al., 2010; Fagan et al., 2013; Gross et al., 2014; 2020; Gross and Joy, 2016; Elardo et al., 2023; Head et al., 2023; Gaffney et al., 2023);
e) identifying magnetic properties of samples to understand the interior structure of the Moon including the life span of a lunar dynamo (e.g., Tikoo et al., 2012, 2017; Wieczorek et al., 2023);
f) helping us recognize lunar meteorites (first meteorite recognized coming from the Moon was Allan Hills A (ALHA) 81004) which are expanding our insights into regions not sampled by Apollo (e.g., Treiman and Drake, 1983; Laul et al., 1983; Delano 1991; Joy et al., 2023);
g) finding exogenic material within the Apollo collection that are shedding light on our solar system dynamics including the timing and delivery of material to the Earth-Moon system at different times in early solar system history (e.g., Day et al., 2006; Cawford et al., 2010; Joy et al., 2012, 2020; Liu et al., 2015; Elsila et al., 2016; Benna et al., 2019; McIntosh et al., 2020);
h) examining changes in solar wind particle production over the last 4.5 billion years (e.g., Nichols et al., 1994; Wieler 2016; McLain et al., 2021), and gaining insights into the location within our galaxy through cosmic X-rays and galactic X-rays (e.g., Simpson 1983; Eugster et al., 1984);
i) providing insights into exoplanet research (e.g., Saxena et al., 2019; Demidova & Badyukov, 2023), and thus, enabling science that goes beyond our own solar system.

Furthermore, Apollo samples are used to develop a greater understanding of crew health and performance on deep space missions, and for performing physical science investigations in the unique lunar environment (e.g., Wagner, 2006; Khan-Mayberry, 2008; James and Khan-Mayberry, 2009; Cain, 2010). Now more than 50 years after Apollo, NASA is returning to the Moon with Artemis and will land the first woman, first person of color, and international partner astronaut on the Moon and will return geologic samples from a different region of the lunar surface than Apollo. Rock, regolith, and core samples to be returned from the surface and subsurface of the Moon during the upcoming Artemis missions are critical to multiple mission priorities, including science, in situ resource utilization (ISRU), and for informing future exploration and long-term Moon to Mars (M2M) goals. Curation will play an instrumental role in helping to prepare for the safe return of these valuable samples, ensuring their integrity during all stages of the missions, including their long-term storage after return, and thus, maximizing their scientific return. As demonstrated by Apollo, Luna, and multiple robotic sample return missions from other destinations, careful and thorough sample curation of collected geologic samples returned to Earth will continue to provide answers to critical science questions decades after they were collected (e.g., Simon et al., 1982; Lentfort et al., 2021; Qian et al., 2021; He et al., 2022; Ito et al., 2022; Fu et al., 2022; Dartois et al., 2023).

During the six Apollo missions to the Moon, 2,196 individual Apollo samples were collected by the astronauts from the lunar surface and subsurface; nearly all of these have been studied to various degrees over the past five decades of lunar science (e.g., Pernet-Fisher et al., 2019; Zeigler et al., 2019). However, six samples were preserved and remained unstudied, unopened, or sealed prior to 2019, with the goal that a subset of these samples would be opened by the next generation of lunar scientists to leverage the world's state-of-the-art laboratory facilities, and thus, enable a multitude of sensitive analyses that were not possible at the time the samples were returned. The six unopened and sealed samples include unsealed drive tube samples 73002 and 70012; sealed drive tube samples 73001 and 69001; sealed bulk soil sample 15014; and frozen basalt sample 71036. Moreover, there was an additional collection of Apollo 17 core and shaded soil samples (70001, 70002, 70003, 70004, 70005, 70006, 70180, 71036, 72320, and 76240) that were initially processed under nominal laboratory conditions in an N_2 cabinet at room temperature, but placed into cold storage (-20°C) within one month of their return to Earth, and that have remained largely unstudied since then.

To prepare for Artemis and the return of new lunar samples, NASA initiated the Apollo Next Generation Sample Analysis (ANGSA) Program for multi-generational consortium studies using the unopened, and unstudied Apollo samples. ANGSA served as a testing ground to understand curation processes, update techniques, and prepare for the preliminary examination (PE) of newly returned samples with Artemis. It was designed to function as a low-cost analog sample return mission in which the consortium used cutting edge techniques to address primary science goals from the Apollo mission. For ANGSA 1.0, nine Principal Investigators (PIs) were selected to study frozen samples and the double drive tube samples 73001 and 73002: Jessica Barnes (University of Arizona), Kate Burgess (Naval Research Laboratory), Barbara Cohen and Natalie Curran (co-PIs; NASA Goddard-GSFC), Darby Dyar (Mount Holyoke College/PSI), Jamie Elsila-Cook (NASA GSFC), David Blake, Richard Walroth, and Jeff Gillis-Davis (co-PIs; NASA Ames, NASA Ames, Washington University St. Louis, respectively), Alex Sehlke (NASA AMES), Charles Shearer (University of New Mexico), and Kees Welton (University of California Berkeley) (for more details see Shearer et al., 2022; Shearer et al., 2024). These PI's led teams of scientists tackling various aspects of Apollo 17 samples but worked together as a larger consortium to attempt to connect the seemingly disparate studies into a coordinated effort. Lessons learned from this effort will help us better prepare for the upcoming return of samples from the Artemis mission.

The first step in the ANGSA sample analyses was the Preliminary Examination (PE) of the samples. PE of returned lunar samples is a science-enabling activity only, and thus, distinct from science (Figure 3) and represents the initial step for ensuring the careful preservation of lunar materials for future research (McCubbin et al., 2019). Prior to PE, basic characterization of these samples took place to document exactly how they existed when their containers were opened (Figure 3). PE involves documenting and characterizing the samples sufficiently to produce an initial sample catalog with sufficient information about the samples that scientists can use it to select and request the most applicable samples for their own research studies. PE ends once the initial sample catalog is released, but extended examination (either through work within the curation office, or ongoing PI studies) results in updates to the sample catalog and is an ongoing process that lasts as long as there are lunar samples remaining in the collection. In addition, when conducting PE, it is critical to find a balance between sample characterization and not conducting scientific research that should be PI-led and competed at a later date. This balance needs to be optimized to minimize unnecessary sample consumption due to a lack of detailed information in the catalog (e.g., using a sample that doesn't contain the necessary components) while still enabling unexpected discoveries within the samples during scientific studies.

Preliminary Examination for 73002 started prior to the COVID-19 pandemic with selected members of the consortium study, but the curation lab was shuttered at the start of the pandemic in mid-March, 2020; after the Apollo curation facility partially reopened in August/September of 2020, PE was performed on 73002 and 73001 with the curation team only. These initial steps in the processing of the core drive tubes represent the first modern dissection of an Apollo core and allow us to prepare for Artemis samples and their return to Earth. Here we focus on the physical history, the process of physical dissection, gas extraction, and the initial characterization of samples 73001 and 73002. The data presented here are the results of the preliminary examination of the samples. Processing of the frozen samples in a N_2-purged environment, including new basalt 71036, will be reported elsewhere.

2. Physical history of double drive tube 73001/73002

The first steps of preliminary examination for crew-collected and returned samples takes place long before they are collected. For 73001 and 73002, the Apollo 17 astronauts Eugene A. Cernan and Harrison H. Schmitt gathered as much data as possible about the lunar surface from where the samples are gathered, including photographs, crew descriptions, and context images of the core location (Feist et al., 2017; https://apolloinrealtime.org/17/?t=144:30:37).

2.1 Collection of 73001/73002 on the lunar surface

Apollo samples 73001 and 73002 were collected in a double drive tube (Allton, 1989) on the presumed landslide deposit on the floor of the Taurus-Littrow Valley, at the rim of Lara Crater and the surface expression of the Lee-Lincoln Scarp during the second Extra Vehicular Activity (EVA) of the Apollo 17 mission (Schmitt et al., 2017). Each drive tube is a hollow, thin-walled aluminum tube, 35 cm long with an inner diameter of 4.1275 cm. These tubes are threated together to form a 70 cm long tube that was hammered into the surface by Apollo 17 astronaut Cernan to record and preserve any potential subsurface stratigraphy and to collect any gasses that may have been emanating from the lunar interior along the Lee-Lincoln scarp. The lower drive tube had a stainless-steel edge magna-formed to the end of it to act as a drill bit that would help drive the tubes into the lunar subsurface more easily (Allton, 1989). After the double drive tube was removed from the lunar subsurface, a small amount of the core material from the bottom of the lower drive tube, 73001, fell out of the core during the recovery process before a Teflon cap could be attached (Butler, 1973). The double drive tube was then separated into two 35 cm long drive tubes by unscrewing them. An unknown amount of material fell out of the bottom of the upper drive tube, 73002, during the securing process on the lunar surface (Butler, 1973). Drive tube with sample 73002 was unsealed, meaning it was just closed, and unbagged. In contrast, the bottom half of the double drive tube, containing sample 73001, was placed in a secondary stain-less-steel tube that had a metal knife edge seal (Indium-Silver alloy), known as a core sample vacuum container (CSVC) (Allton, 1989); no additional material was lost during this process than the material lost during removal from the subsurface. This CSVC was sealed under vacuum on the lunar surface and each individual drive tube sample was secured in the Apollo Lunar Sample Return Container #2 (ALSRC or short Sample Return Container [SRC] aka “rock box”) (Butler, 1973). ALSRCs were sealable boxes machined from blocks of aluminum and lined with woven aluminum as padding (York mesh), and once filled were sealed on the lunar surface for the trip back to Earth. Other samples, such as rocks, rake samples, and regolith samples, were placed in Teflon bags, closed, and stored in sample collection bags (SCB) which were carried by the astronauts. After launch from the surface and prior to transfer of the SCB's from the Lunar Module (LM) to the Command Module (CM), each SCB was put into a Beta cloth decontamination bag to keep the lunar dust adhering to the outsides of the return container from dirtying the inside of the Command Module. Only the samples in sealed containers (ALSRCs, the CSVC, and the Special Environment Sample Container- SESC) were not exposed to spacecraft and terrestrial atmospheres during transit to Earth and recovery on Earth (Butler, 1973). Most of the non-sealable containers (such as SCBs) were tightly closed, but circulation of spacecraft atmospheres was probably enhanced by de-pressurization and re-pressurization on the Moon and in space (Butler, 1973).

2.2 Recovery and transport to the Lunar Receiving Laboratory (LRL)

After splashdown, the command module was recovered and loaded on the recovery vessel U.S.S. Ticonderoga and the sample return containers were retrieved from the command module. Although conditions of both ALSRCs and most of the decontamination bags was nominal, one of the Beta cloth decontamination bags, stowed on the floor of the command module, was completely soaked as it lay for 10 hours in 1/4 inch of water (Butler, 1973). It is unclear if the water was from condensation inside the CM or sea water that splashed into the module during crew recovery. Thus, after recovery from the CM, all the SCB's were removed from the decontamination bags and all the return containers were individually bagged in two layers of Teflon bags and one polyethylene bag, which were heat sealed in an isolated work area on the recovery vessel that had filtered air. These bagged containers, along with the ALSRCs, were then placed in padded crates and transported to the Lunar Receiving Laboratory (LRL) at NASA Johnson Space Center (JSC) by aircraft, arriving in Houston within 24 hours of splashdown.

2.3 Handling and storage in the lunar curation facilities on Earth

On receipt of the containers in Houston, the exterior of ALSRC #2 was cleaned, and a pressure of 28 microns Hg (i.e., 2.8 x 10^{-2} torr) was measured, which suggested it was mostly successfully sealed on the lunar surface (lunar surface pressure ~10^{-12} torr). The ALSRC was then moved into the sample nitrogen atmosphere processing (SNAP) line for opening.

2.3.1 Sample 73002

Sample 73002 was removed from the ALSRC inside the nitrogen purged processing cabinets, its mass by difference recorded (430 g), and triply sealed in Teflon bags within that environment. The bagged sample was taken to a medical X-ray scanning facility at JSC in early 1973 to image the material inside the tube. The radiographs showed the length of the regolith material within the tube was approximately 23.5 cm, though numerous void spaces were also observed (Figure 4). After these scans, the still-bagged 73002 drive tube was placed into special storage within the nitrogen purged cabinets at JSC and left untouched. Eventually 73002 was one of the samples transferred for storage in nitrogen purged cabinets at the Apollo remote storage facilities at Brooks Airforce Base (1976-2002) and White Sands Test Facility (2002-2019).

In the spring of 2019, the sample was returned to Johnson Space Center (transported bagged with a nitrogen atmosphere) in preparation for the ANGSA program and stored in a nitrogen purged cabinet within the lunar vault. In the fall of 2019, the Teflon bags surrounding 73002 were briefly opened within the Apollo nitrogen purged processing cabinets and the material within the tube was more securely immobilized using a specially designed materials compliant tool; this resulted in the overall length of the regolith material being compacted to ~20 cm (based on whole core XCT scanning; see section (2) below). The sample was then triply resealed in Teflon bags. Sample 73002 was transported to the High-Resolution X-ray Computed Tomography (XCT) facility at The University of Texas at Austin (UTCT) in October 2019 where a series of XCT scans were performed on the bagged sample (see section (1) below) (Figure 4). Upon completion of the XCT scans, the sample was returned to secure nitrogen-purged storage in the lunar vaults until the sample was extruded and processed starting in November of 2019 (see section (3) below).

2.3.2. Sample 73001

Upon return to Earth, sample 73001 (in the unopened CSVC) was removed from the ALSRC inside the nitrogen purged processing cabinets, mass (by difference) was recorded (809 g), and then the CSVC was sealed within a large outer vacuum container (OVC) made of stainless steel with an aluminum gasket that was pumped down to ~10^{-2} Torr, which was then, in turn, sealed inside two large Teflon bags. The OVC was placed in special low-vibration nitrogen purged storage in the lunar curation facility. In the spring of 1976, it was suspected that the valve on the OVC was leaking, so the valved flange was removed, replaced with a new valved flange, and the OVC was again pumped down to an atmospheric pressure of 10^{-2} Torr. All this work was carried out inside the nitrogen purged cabinets to avoid contamination with terrestrial air. After the OVC repair, 73001 sat inside its never opened CSVC, repaired OVC, and two outer Teflon bags, undisturbed in low vibration nitrogen purged storage in the lunar vaults for 46 years until it was removed for gas extraction, XCT analysis, and extrusion/dissection, and thin section preparation starting in March of 2022.

3. Initial characterization and preliminary examination (PE) of samples 73002 and 73001

Sample 73002 was the first Apollo drive tube sample to be opened in over 25 years. Therefore, all the equipment that was needed for the extrusion and dissection process had to be located, cleaned, assembled, and tested (including procurement of replacement parts where needed) over a period of ~12 months. A similar process was undertaken to renovate and rebuild the entire core vacuum impregnation and curing devices for making continuous core thin sections at the end of the dissection process. In addition to the hardware upgrades, the procedures for sample dissection had to be reviewed and modernized, which included building a full-sized cabinet mock-up and extensive testing with analog samples (Krysher et al., 2020). The preliminary examination (PE) of sample 73002 began in November of 2019 and concluded in December of 2021 (25 months). The protracted nature of the PE was almost entirely due to laboratory access issues related to the COVID-19 pandemic. The PE of sample 73001 began in March of 2022 and concluded in October 2022 (~7 months). The steps in the PE process, and the detailed work within each PE step, were similar for samples 73001 and 73002; the only notable exception was the gas-extraction process that was necessary for sealed sample 73001, but not for unsealed sample 73002. PE steps included:

- 73001: (1) XCT scan of bottom portion of the drive tube; (2) Gas Extraction; (3) Whole Core XCT; (4) Extrusion and Dissection of Regolith Materials; (5) XCT of >4 mm individual particles
- 73002: (1) N/A; (2) N/A; (3) Whole Core XCT; (4) Extrusion and Dissection of Regolith Materials; (5) XCT of >4 mm individual particles

3.1 PE Step 1: XCT scan of bottom part of the drive tube 73001 prior to gas extraction.

Prior to piercing and extracting gas from the CSVC that held the 73001 drive tube, an XCT scan of the bottom portion of the CSVC was collected to confirm the state and location of the Teflon cap attached to the bottom of the 73001 aluminum drive tube, to measure the space between the CSVC bottom and the Teflon cap of the drive tube, and to verify the stainless steel wall thickness of the CSVC. The scan was performed out at the Astromaterials X-ray Computed Tomography Laboratory at Johnson Space Center using a Nikon XTH 320 system with a 225 kV rotating reflection target source at 215 kV, 153 μA, and a 32.57 μm/voxel resolution. This information was essential to confirm that the European Space Agency had accurately designed and constructed the piercing tool needed for gas extraction (McDonald et al., 2022; Schild et al., 2022).

3.2 PE Step 2: Gas extraction of 73001

As part of the ANGSA program, the gas in both the 73001 OVC and CSVC was extracted (Figure 5). The OVC had an external valve in place to help facilitate gas extraction, but the CSVC did not have an external valve. Thus, the CSVC had to be pierced to extract the gas (similar to a keg being tapped). Gas extraction was achieved using two bespoke pieces of equipment that were specifically built for the ANGSA project: (1) a gas extraction manifold built by the Team at Washington University in St. Louis led by Drs. Alex Meshik, Olga Pravdivtseva, and

Rita Parai; (2) a piercing device built by a team at ESA led by Dr. Francesca McDonald. Gas was extracted from the OVC and CSVC using differential pressure between those containers and the gas extraction manifold, which typically achieved pressures in the mid 10^{-9} Torr range (unless otherwise noted). The gas extraction manifold originally had eight ~2-liter stainless steel bottles and two 50 cm^3 stainless steel bottles attached to it for storing the extracted gas; a ninth ~1-liter stainless steel bottle was also added to the system before the extraction was completed (Figure 5a). See Table 1 for a summary of all gas samples acquired.

Two separate gas extractions from the OVC were done (Figure 5). The initial OVC extraction was done with a background manifold pressure of 4 x 10^{-6} Torr, an equilibration time of 15 minutes (all equilibration times are 15 minutes unless otherwise stated), and the gas was expanded into one 2-liter bottle and one 50 cm^3 bottle. The equilibration pressure observed on gas sample OVC1 was 28 Torr. Just prior to acquiring gas sample OVC1, a system blank was collected under the sample conditions (e.g., similar background manifold pressure and equilibration time). The second OVC extraction was collected into one 2-liter bottle with a background manifold pressure of 5 x 10^{-8} Torr; the gas for OVC2 was passed through a tube sitting in a water ice bath during extraction (Figure 5a). The equilibrated pressure on OVC2 was 7 Torr.

After the OVC gas extraction was completed, the OVC was placed back into the N_2-purged curation cabinets, the OVC was opened, the CSVC was removed from the OVC, and the CSVC was sealed within the piercing tool (Figure 5b). The piercing tool was then removed from the N_2-purged cabinets and connected to the gas extraction manifold (Figure 5c). The piercing tool was then pumped down by the gas extraction manifold prior to piercing the CSVC to remove the N_2 cabinet gas in the piercing tool. During the pump down of the piercing tool over the course of ~48 hours, we were unable to achieve a manifold pressure lower than 10^{-6} Torr, whereas we could achieve a vacuum of 10^{-9} Torr in the manifold when the piercing tool was isolated. The residual gas analyzer (RGA) analysis of the gas being pumped out of the piercing tool appeared to be nearly pure N_2 gas and showed no evidence for atmospheric contamination of the system, nor did multiple He-leak checks of the piercing tool and extraction manifold show evidence of an external leak. Thus, it was decided that there was a slow leak of the CSVC bleeding gas out into the piercing tool.

The CSVC "leak gas" was accumulated within the piercing tool for ~24 hours and then collected into one 2-liter bottle with a background manifold pressure of 10^{-9} Torr (CSVC Leak Gas 1). This process was repeated under almost identical conditions to collect an additional 2-liter bottle of gas as CSVC Leak Gas 2. In both cases, the observed equilibration pressure in the collection bottle for the leak gas samples was ~0.2 Torr. After the CSVC leak gases were collected, the piercing tool was isolated from the manifold, the piercing mechanism on the piercing tool was successfully used to pierce the bottom of the stainless steel CSVC (making a ~2 mm hole), and a first gas extraction from the pierced CSVC was collected in two 2-liter bottles and one 50 cm^3 bottle (CSVC1) with an equilibration pressure of 4.6 Torr. A second longer gas extraction (CSVC extraction 2) was performed with an equilibration time of 10.75 days, with a final equilibration pressure of 3.2 Torr. Finally, the gas extraction manifold was used to pump down the CSVC/piercing tool to a pressure of 2×10^{-7} Torr. The piercing tool with the pierced CSVC inside was then closed off for 6 days so that the remaining gas from the CSVC could expand into the piercing tool, and a final CSVC extraction 3 was collected into a single 2-liter bottle with a final equilibration pressure of 5×10^{-4} Torr.

The two 50 cm^3 bottles of gas (OVC1; CSVC1) were subsampled and portions of each distributed for preliminary analyses to ANGSA Team members Dr. Zachary Sharp at the University of New Mexico and Dr. Rita Parai at Washington University in St. Louis. Dr. Sharp's results showed that the vast majority of gas within both the OVC and CSVC is N_2, and thus there is little evidence for laboratory atmosphere contamination within the samples. The $\delta^{15}N$ value of -4.4‰ relative to air, generally consistent with the gas used in our N_2 purged cabinets but suggesting that ^{14}N has preferentially leaked into the system from the cabinet. The CSVC sample has a lower absolute concentration of N_2 than the OVC sample (98.3% vs. 99.9%), suggesting that some of the H_2O, H_2, and Ar within the CSVC could be indigenous to the sample, although some of the H_2 would have exsolved from the stainless steel over the years of storage (e.g., Rezaie-Serej and Outlaw, 1994). Similarly, Dr. Parai's results for major gas phases measured by RGA showed that N_2 was the dominant gas (presumably curation cabinet gas), with measurable CO_2 and H_2 gas (likely exsolved from the stainless steel containers), and no evidence of significant contamination of the OVC or CSVC gas from laboratory air. Although there was some evidence of a terrestrial component in some of the noble gas measurements from the CSVC-1 sample, there was also clear evidence of a solar wind component apparent in both the Ne and Ar isotopes. For more details on the results see Parai et al. (2022) and Sharp et al. (2022). Currently, all nine 1-liter or 2-liter bottled gas samples listed in Table 1 are attached to the gas extraction manifold, which is being maintained at low 10^{-9} Torr pressure (Figure 6). Each bottle is double valved with a "between valve" volume of ~37 cm^3 so that requesting PIs can bring their own pre-conditioned gas sample bottles for allocation of gas samples.

3.3 PE Step 3: Whole core XCT scanning

Prior to extruding the regolith material from drive tubes 73001 and 73002 (see section 3.4 below), each sample was scanned by XCT at the University of Texas High-Resolution X-ray Computed Tomography (UTCT) Facility (Figure 7; Zeigler et al., 2021, 2022; Ketchum et al., 2022; Eckley et al., this volume). This was done to: (1) facilitate non-destructive, rapid detection of minerals, lithic clasts, and void spaces within the drive tubes in order to identify any potential complications during the extrusion or dissection process; (2) determine the pre-extrusion length of the tube to better inform the overall sampling depth of the core; and (3) to establish a permanent record of any potential stratigraphy and clast locations prior to extrusion – and thus the loss of such record –, for more in-depth studies after PE was concluded. The pre-extruded length of the 73001 core was measured at 34.9 cm and the pre-extruded length of the 73002 core was measured at 20.1 cm based on the XCT scans.

Prior to the whole core scan at UTCT, the bottom of the 73001 CSVC was scanned again as well as the top of the 73001 CSVC by XCT at NASA JSC (Figure 8) after the gas extraction. The bottom scan was done with the same settings as the pre-gas-extraction scan and the top scan was done at 215 kV, 179 μA, and a 38.5 μm voxel size. The purpose of these preliminary "engineering" scans were to: (1) characterize the nature of the piercing hole at the bottom of the tube and to evaluate the effectiveness of the piercing tool; (2) determine if the Teflon cap, which secures the lunar soil when the aluminum drive tube is removed from the CSVC, was damaged; (3) confirm that the regolith at the top of the core was properly immobilized; and (4) image the In-Ag metal-knife edge seal on the CSVC prior to opening in case this information was needed for future tool design (e.g., Artemis). The scan of the bottom of the 73001 CSVC confirmed that the piercing tool worked as intended (Figure 8b), the hole made by the piercing device was large enough to permit gas to freely flow (orange arrow in Figure 8b), and that the Teflon cap on the bottom of the 73001 aluminum drive tube was undamaged and securely in place (dark yellow arrows in Figure 8b). The scan of the top of the 73001 CSVC however, showed that the tube was overfilled, and thus the part of the tube apparatus designed to keep the regolith in place (the keeper) was not properly seated in the tube (Figure 8a). Instead of deploying and pushing the keeper inside the drive tube (with an inner diameter of 4.1275 cm), where its prongs catch the walls and lock in place (blue arrows in Figure 8a), thus restraining the regolith from moving, the keeper sat on the widest part of the drive tube with a diameter of 4.415 cm, too wide for the pongs to come into contact with the walls (Figure 8a). The screw of the CSVC sealing mechanism was the only element holding the keeper, and thus the lunar regolith, in place. Therefore, instead of removing the drive tube from the CSVC before the transport to UTCT for XCT scanning as initially intended, the CSVC was left intact so that 73001 could be safely transported and its stratigraphy could be preserved. With this new initial information, a modified extrusion plan was derived to ensure sample integrity during the extrusion process with a compromised keeper in place, while the sample was being scanned at UTCT. These initial scans of the top and bottom of the CSVC were critical in the successful piercing, gas extraction, whole-core scanning, and extrusion of 73001.

The whole core XCT scans from 73001 were taken through the stainless steel of the CSVC, the aluminum drive tube, and three Teflon bags in which the CSVC was sealed within the nitrogen purged atmosphere of the JSC curation processing cabinets. The whole core XCT scan of sample 73002 was taken through the aluminum drive tube that had also been triply bagged in Teflon within the nitrogen purged processing cabinets (Figure 7). Both samples were scanned at UTCT using a Feinfocus FXE 225.48 microfocal X-ray source and a 2048x2048 Perkin Elmer XRD 1621 N ES flat panel detector. To achieve maximum spatial resolution, the NSI Subpix^{TM} capability was used, in which four overlapping data sets are gathered with half-pixel vertical and horizontal offsets of the detector, virtually doubling the detector size to 4096x4096. Sample 73002 was scanned mounted vertically in a plexiglass tube, with X-rays at 180 kV and 180 μA and pre-filtered with 0.72 mm Al. Sample 73001 was mounted similarly, however X-ray energy was increased to 190 kV and 180 μA with no filter.

Data were acquired as a series of six (73002) and nine (73001) individual cone-beam volume scans, with overlap (~500 slices) to aid in stitching them together to create a continuous data set for each core. The voxel resolution on all scans was 12.9 microns. There are 27,600 slices in the finished 73001 scan and 15,800 slices in the finished 73002 core scan. Each individual scan was corrected for uneven beam and isometric distortion in Z using a linear rescale for both CT value and geometry across Z (i.e., per-slice basis; central slice used as geometric standard). The different scans were then geometrically matched (rigid translation and rotation). For the initial distribution of data from 73002, CT values in each scan were rescaled (second degree polynomial) to match the spot directly 'below' (e.g., scan 2 matched to scan 1, etc.). Seams between scans were then blended using a gradual linear combination of 9 (73002) and 80 (73001) overlapping slices centered at the matching reference slice. The CSVC, as well as the stainless-steel bit embedded in the 73001 Al-drive tube both caused considerable artifacts in the initial XCT data, and great effort was made to develop specific corrections for those effects; these corrections led to further processing of the 73002 scans to maximize data consistency for subsequent image analysis (see Ketcham et al., 2022 and Eckley et al., this volume, for more detail).

The fly-through videos of both the whole core 73001 and 73002 scans (at down-sampled resolution of 51.6 µm/voxel), as well as fly-through videos of the engineering scans taken at the top and bottom of the 73001 CSVC (38.5 µm/voxel) can be found in Appendix 1 on the lunar curation website (https://curator.jsc.nasa.gov/lunar/angsa_catalog.cfm). In these videos, the brightness of different phases are a result of the attenuation of X-rays by that phase, which is a function of the density and average atomic number of the phase, as well as X-ray energy. Brighter phases have higher density and/or atomic number. Although it does not represent the same phenomenon, the effect is very similar to that observed in back-scattered electron images. Although XCT scans do not provide primary mineralogical information, for lunar samples, the relative brightness of phases almost always follows the sequence (increasing brightness): void space, silica phases; feldspar; pyroxene; olivine; FeTiCr oxide; Fe sulfides; FeNi metal and stainless steel. There can be overlap between adjacent phases in this list, especially for phases which have considerable Mg-Fe substitutions (e.g., pyroxene and olivine).

3.4 Step 4: Physical dissection process

3.4.1 Extrusion process

The extrusion and dissection of both 73001 and 73002 took place in the core processing cabinet in the pristine Apollo sample laboratory facility. Sample 73002 was processed first, from November 2019 till December 2021, and sample 73001 was processed from March 2022 till June 2022. The cabinet, equipment, and tools used during extrusion and dissection were cleaned using our in-house cleaning facility following our standard protocols prior to each sample. The only exception was that all materials to be introduced into the core processing cabinet were entirely bagged in Teflon (normal Apollo sample processing uses nylon bags for tools and consumables). Three separate Si-metal and one baked-out Al-foil witness materials were deployed in the core cabinet for each dissection prior to insertion of any equipment, kept out during the entire process, and preserved after PE finished, as a record of the exposure history of the initial processing of the core samples.

The standard Apollo sample processing procedures are designed to minimize all types of contamination into the Apollo processing cabinets, but they were developed with inorganic cleanliness foremost in mind. One of the primary goals of the ANGSA program was to measure the organic components of 73001 and 73002 (i.e., Elsila et al., 2024). To minimize the introduction of organic or biologic materials into the cabinet during processing, extra care was taken when introducing new materials into the processing cabinet: (1) the airlock was cleaned out with alcohol wipes every third time it was used (cleaning the airlock every third time proved to minimize organics, and additional cleaning did not improve cleanliness levels); and (2) an additional smock and nitrile gloves were worn on top of the normal clean room gear. The core processing cabinet was monitored for microbial contamination prior to loading each core and after the dissection was completed (and the core removed). The cabinet airlock and core room flooring were tested once a month during the dissection process to understand biological contamination in the vicinity as well. The testing results showed that the cabinet remained abiotic throughout the extrusion and dissection of 73001 and 73002 (Regberg et al., 2021; Elsila et al., 2022, 2024).

The extrusion (Figure 9) and dissection process for core samples 73001 and 73002 occurred in several steps, and was identical for both core samples, except for step 1 below, which was only necessary for 73001 (because it was in a CSVC).

1. Sample 73001 was removed from the CSVC. During the process of removing the sample, a small amount of material fell out of the very bottom of the drive tube. This material was preserved as "interval 67", representing the lowermost ~0.5 cm of the 73001 core.
2. The ends of the drive tubes were removed, and special end effectors were added to aid with the extrusion process. These modified drive tubes were then mounted into extrusion hardware (Figure 9c) that was aligned with a receptacle, and slowly extruded from the drive tube into the receptacle, which consisted of an aluminum base that has removeable aluminum plates, with a quartz top (Figure 9d). The post extrusion length of 73001 was 33.1 cm and the post extrusion length of 73002 was 18.5 cm.

3.4.2 Physical dissection:

After extrusion into the receptacle (Figure 9), the aluminum base with the extruded core and quartz top (Figure 9b) were carefully lifted onto the dissection table, and the quartz top was removed from the core. Because the regolith was in contact with the aluminum core tube and quartz top, the first step in the dissection process is to "de-rind" the core. This is achieved by removing the outmost 1-2 mm of material to expose the underlying pristine material (Figure10). De-rinding was done in 5 cm intervals.

Each core was dissected in three passes: Pass 1, Pass 2, and Pass 3 (Figure 10). A pass accounts for approximately 1/4 of the material in the core (a pass is about 1 cm "tall"). Each pass was subdivided into intervals that are each 0.5 cm wide, starting with the side of the core that was closest to the lunar surface. Each interval represents a unique depth within the core, and the same interval in different passes represents the same depth (i.e., Pass 1, interval 27 and Pass 2, interval 27 are from the same depth beneath the lunar surface). 73002 has a total of 37 intervals, while 73001 has a total of 67 intervals. After each pass was dissected down to plate level (Figure 11), two plates were removed from the table so that the core stuck out ~1 cm above plate level again (Figure 11a). The sides were then de-rinded to expose the pristine material, and the pass dissected afterwards in the same manner as the previous pass (Figure 11b).

The material removed from each interval in Pass 1 and Pass 2 were collected onto a pan and sieved into <1 mm fines and >1 mm particles. The >1 mm particles were manually subdivided into the following size fractions: 1-2 mm; 2-4 mm; 4-10 mm; and >10 mm particles (Figure

11c). All particles were sorted into their respective size fraction onto a Teflon pad and photographed from multiple angles and different lighting conditions to best capture their shape and color shade, although nearly all particles are mostly or entirely obscured by adhering dust. All particles >4 mm (352 total) were individually triple bagged in Teflon (Figure 11c) and scanned by XCT at NASA JSC (see section 3.5 below). Pass 3 is considered the most chemically clean portion of the core since it was the farthest from the tube, and thus, the intervals in Pass 3 were not sieved, though particles >10 mm were removed using stainless steel tweezers.

Each size fraction from each interval was given a unique subsample number, placed inside individual stainless steel and Teflon containers, and weighed. The mass of each subsample is recorded in the Apollo sample database. The subsamples are in stainless steel racks that are sealed in Teflon Bags and stored in the nitrogen purged Apollo sample cabinets. An inventory spreadsheet was created (Figure 12) that contains the general information of each pass and each interval including: (1) dissection date; (2) depth of the interval within each core; and (3) total interval mass. In addition, the spreadsheet contains: (1) the number of particles in each (>1 mm) size fraction; (2) the mass of each size fraction; (3) the percent of sample mass per size fraction; (4) the parent number of each size fraction; and (5) the individual information about each particle that was >10 mm (e.g., if XCT scanned, its individual weight, name/number, origin, etc.) (Figure 12). The inventory spreadsheets for 73002 and 73001 can be found on the Lunar Curation Website, Appendix 2 (https://curator.jsc.nasa.gov/lunar/angsa_catalog.cfm).

Detailed photographs and notes were taken to document the dissection process (Figure 13). The Processing photographs can be found on the Lunar curation Website, Appendix 3 (https://curator.jsc.nasa.gov/lunar/angsa_catalog.cfm). Variations in core properties were noted and recorded (Figure 13a), such as changes in grain size, color, compactness, looseness, friability, clast locations, etc. For 73002 Pass 1, detailed sketches were made for each dissection interval and later digitized (Figures 12, 13), for later passes in 73002 only rough sketches were taken but not digitized, and in 73001 this step was omitted due to time constraints. At the end of each dissection pass, the full core was photographed with a colored chart to create a permanent record of each dissected surface and best capture any changes. The images taken during the dissection of core samples 73001 and 73002 as well as the processing notes taken during the dissection of core sample 73002 can be found on the Lunar Curation Website, Appendix 3 & 4 (https://curator.jsc.nasa.gov/lunar/angsa_catalog.cfm).

During the dissection process, several non-standard dissection procedures were implemented such as time-sensitive sampling for organics and bulk D/H ratio measurements on Pass 1 of both 73001 and 73002 (i.e., they were dissected “out of order”) (Elsila et al., 2022a,b; Sharp et al., 2022; Welton et al., 2022), and mm-scale subsampling of a portion of the top two intervals on Pass 3 of 73002 (Welton et al., 2022).

3.4.3 Multispectral analyses of 73001/73002

After de-rinding and after each pass (1-3) was dissected down to plate level, multispectral measurements of 73002 and 73001 were taken by placing a spectrometer built at the University of Hawaii on top of the core cabinet (Sun et al., 2021b). The cabinet glass is comprised of borosilicate, so spectral measurements are limited to visible and near-infrared (400-2500 nm) wavelengths. This multispectral imager comprised a monochrome imaging camera, a 6-position motorized filter wheel equipped with 6 narrow band interference filters, lenses, and light source. The center wavelengths of the six filters were: 415 nm, 570 nm, 750 nm, 900 nm, 950 nm, and 990 nm. These wavelengths share some of the bands used by the Clementine UVVIS camera, the Lunar Reconnaissance Orbiter Camera Wide Angle Camera, and the KAGUYA Multiband Imager and allow for direct comparison of the dataset produced from the core to datasets produced from orbital observations of the lunar surface. Both cores 73002 and 73001 were scanned at a spatial resolution of 60 μm after each pass. This process required the Apollo lab to be darkened for the time it took to scan the dissected core surface, so that the only light source came from the multispectral imager itself.

In addition to the scans after each pass, 73001 offered a unique opportunity to spectroscopically examine soils that have been curated differently (stored under vacuum) than other drive tube samples from the Moon. To assess the state of water or hydroxyl in this sample that may represent the state of hydration on the lunar surface, 73001 was scanned via Fourier Transform Infrared (FTIR) spectroscopy. After the last multispectral measurement of pass 3, and immediately prior to removal of 73001 from a nitrogen environment for epoxy impregnation and thin section production, a portable FTIR spectrometer (with a spectral range from 2 to 14 μm) was used to collect spectra from the dissected surface inside the nitrogen purged curation cabinet. Spectral measurements were made (1) shortly after introducing the spectrometer into the cabinet, (2) the next day, and (3) three hours after the pristine cabinet was vented to room air. For details and results, see Sun et al. (2021) and Lucey et al. (2023).

3.4.4 Continuous core sections

After dissection was complete, the last portion of core remaining in the dissection table (about ¼ of the overall core material) was taken to the Apollo thin section laboratory and impregnated with a mixture of Araldite-506 epoxy (resin), aminoethyl piperazine (hardener), and butyl glycidyl ether (thinning agent and curing retardant) (Figure 14). Impregnation was done at a vacuum pressure of 3 torr to allow full penetration around the core's submicron dust particles and expel the gases formerly present within the core. The purpose of this process is to preserve a record of the stratigraphy of the core and the location and orientation of particles within the core. The epoxy also helps to stabilize the core and avoid fragmentation, crumbling, and plucking during cutting and polishing, as well as to fill few void spaces that were left behind from larger clasts that partially extended into this last ~¼ of the core and were removed during the prior dissection process. After the epoxy mixture was added and bubbles stopped coming out of the core, the vacuum was released, and the core was transferred to an incubator where it cured for several weeks under low humidity (< 35 %) at 45 ˚C (Figure 14a). Following the complete cure, the epoxy impregnated regolith material was removed from the dissection plate (Figure 14b) and a secondary epoxy layer was added around the core to encapsulate and protect it more fully (Figure 14c). This secondary encapsulation epoxy did not include any added butyl glycidyl ether and instead incorporated diamino-p-menthane as a reaction catalyst. The silicone mold used for this secondary encapsulation included a scale and orientation markings to aid in precise cutting of the core at a later point. The secondary encapsulation cured for another 2 days and was then sawn in half along the long axis of the core, using ethanol as the cutting fluid. One of the two halves was then further sawn into 4 to 5 cm long potted butts (4 potted butts for 73002; 8 potted butts for 73001) using the previously added scale (Figure 14d). Two sets of continuous standard rectangular thin sections, with a standard thickness of 30 microns, were made down the length of the core for both 73001 (= 16 thin sections) and 73002 (= 8 thin sections) using these potted butts. The left-over material of the potted butts can support several additional thin sections per potted butt and are curated for future thin section needs of the core.

3.5. Step 5: Individual particle XCT

Each of the >4 mm particles in 73001 and 73002 that were separated, and triple bagged in Teflon as part of the dissection process (see details in 3.4.2 above) were individually scanned via XCT at NASA JSC using a Nikon XTH 320 with a 180 kV W transmission target source. 132 particles were scanned from 73002 at x-ray energies ranging from 90-155 kV and 18-39 μA and resolutions from 2.8-20.6 μm/voxel. 220 particles were scanned from 73001 at x-ray energies ranging from 90-145 kV and 33-37 μA and resolutions from 2.8-22.6 μm/voxel. For each particle the following data were produced: (1) a fly-through video; (2) a description of the main features in the particle, recorded in the data table (Lunar Curation Website, Appendix 5: https://curator.jsc.nasa.gov/lunar/angsa_catalog.cfm); and (3) a preliminary lithologic classification (Figure 15) based on the features observed. The particles of 73002 and 73001 fall into the following preliminary lithologic categories, respectively (Figure 15, 16a,b): agglutinates (n_{730002} = 6; n_{730001} =1); anorthosites (n_{01} =1); granulites (n_{01} = 2); impact melts (n_{02} =5; n_{01} = 2); impact-melt breccias (n_{02} = 42, n_{01} =115); high-Ti basalts (n_{02} = 9; n_{01} = 28); low-Ti basalts (n_{02} = 4; n_{01} = 3); regolith breccias (n_{02} = 62; n_{01} = 64); and soil breccias (n_{02} = 2; n_{01} = 1). In addition to the main lithologic category, an attempt was made to recognize some sub-groups of particles that shared similar characteristics, primarily among the impact-melt breccias (e.g., the poikilitic ilmenite group). Because the lithologic determinations were made using only the XCT information, they are not intended to be (1) the final determination of the lithology of each fragment, but rather serve as a guide for investigators to request particles for follow up analysis; and (2) overly specific, placing samples into broad lithologic categories based primarily on suspected mineral abundances, with less weight given to other factors (e.g., texture). See Table 2 for more details about the classifications. The fly-through videos of each scanned particle can be found on the Lunar Curation website, Appendix 6 (https://curator.jsc.nasa.gov/lunar/angsa_catalog.cfm). See Eckley et al. (this volume) for more details on XCT scans of the particles.

4 Discussion

4.1 Timeline of physical dissection of 73002 and 73001

Dissecting a core takes time. It depends on multiple factors, including but not limited to the physical properties of the core, its compaction, the training of the processors, external events (e.g., pandemic with associated restricted access to laboratories), unexpected challenges, hardware delivery (e.g., clean dissection tools), length of the core, processing days, disturbances in the lab, etc. Individual intervals are 0.5cm in width and take between 20 - 40 min of careful and meticulous dissection depending on the physical behavior of the core (e.g., if there is a lot of slumping it takes longer). The collected regolith then gets sieved, which takes about 5 min; the >1 mm clasts are then picked up from the sieve with tweezers and carefully transferred onto a Teflon Disk and sorted into different size fractions. The picking and sorting process depends on the quantity of clasts in each interval but on average takes an additional 10 - 15 min. Afterwards, the dissected core surface as well as the sorted clasts are photographed and documented using different lighting conditions and different image angles to capture the true nature of the regolith. The photo-documentation process takes up to 15 min. After documentation is finished, each size fraction is placed inside its own sample container, counted, weighed, the weight documented, and then placed inside a core rack. The counting/weighing process takes about 15 min per size fraction. The >4 mm particles are weighed individually and then triple bagged in Teflon bags, a process that takes about 25 min per particle. Thus, dissecting an individual interval can take up to 3 hours. This does not include the documentation, transcribing, annotating, digitizing of all notes, images, entering information into the databases, and completing internal curation forms to track the handling history of all samples during dissection, transfer, allocation, and storage, an overall process that can take up to 2 days per interval. With these processing times and documentation, it takes about 6-8 months to carefully dissect a core.

4.2 Data connectivity and importance

Documentation during the preliminary examination, during the extended examination, and during long term curation is an extremely crucial process to maximize the scientific return of the samples. Documentation includes notes, sketches, annotated images, weights, and instrument data such as XCT scans during PE and extended PE, as well as the handling history of the samples while in transit to or from the various laboratories used for PE, inside instruments (such as XCT scanner, Secondary Electron Microscope) and ultimately while with principal investigators at their respective facilities. To track all the different data products generated during ANGSA PE, numerous data tracker/recording systems were created that are tailored to each type of data being hosted and that are all linked to each other through an internally consistent naming scheme (Figure 12). These trackers include:

1) Images, that contains PE images generated during processing to document the dissection process. Images are sorted into different passes, respectively. Full core images with a colored bar and a scale were taken at the end of each dissection interval under various lighting conditions to best capture color and color variation within the dissected core surface.

2) Particle images, which includes images of the clasts sorted into different size fractions on the Teflon disk with a scale. These particles were photographed from several different angles and lighting conditions to capture their shape and color more accurately.

3) XCT particle data; this data includes representative 2-D slices and full XCT videos of all > 4mm clasts. This information was used for classification of particles.

4) An inventory excel spreadsheet, which includes information about each interval in each pass per sample. Information captured in this inventory includes interval dissection dates, interval information such as pass, interval number, interval size, depth, and total mass; number of clasts per size fraction in each interval; mass of each size fraction; percentage of mass per size fraction; parental numbers of all > 4 mm particles and each size fractions; all > 4 mm clast names, their individual mass, and whether the particle was XCT scanned or not.

5) Notes and dissection sketches of each interval for 73002, pass 1 & 2 and notes only for 73002 pass 3 and all of 73001. These data record changes and characteristics within the core that might be otherwise missed, such as the feeling of compactness during physical dissection, slumping/collapsing behavior of core/intervals, identity of curation personnel and visitors present, weight of size fraction per interval (recorded for redundancy), any clast characteristics noteworthy such as size, shape, coloration, “sparkle”; behavior of the soil during sieving (aka stickiness), etc.

These data products are all linked to each other through an internally consistent naming scheme that allows one to easily track each particle and any information pertaining to the particles within each interval (Figure 12). These linked datasets provide the scientific community with an easy and consistent record from which to select the best and most appropriate material for their respective studies. As such, the particles in the particle images data products are labeled sequentially starting with A for the first particle, B for the second, etc., which is tracked with the same identifier in the inventory excel spreadsheet. The 2D image slice file and 3D video files of the XCT scans of all > 4 mm particles are named with the same sample numbering scheme (Figure 12).

4.3 Grain size analyses with depth

The inventory data tracker/recorder allows for fast and easy comparison of different characteristics with depth of the core such as horizons in which clasts could be concentrated. Data from pass 1 and pass 2 data for 73002 and 73001, respectively, were combined to show any potential variations or concentration horizons with depth. Pass 3 was not included as those passes are considered chemically clean, and thus, were not sieved. Therefore, no grain size analysis exists for pass 3 in 73002 and 73001 except for >10 mm clasts. While some intervals contained fewer large particles, no systematic trend could be detected (Figure 17). Analyses of the grain size (<1 mm, 1-2 mm, 2-4 mm, 4-10 mm, and >10 mm) volumes per depth interval did not show any concentration horizons or otherwise preferred orientation (Figure 17).

4.4 Compaction within the core

Samples 73001 and 73002 were compacted several times from collection on the lunar surface to the end of extrusion within the Curation Facility at NASA JSC. The first time the regolith within the drive tubes were compacted took place on the lunar surface during/after collection. During the placement of the keeper, which keeps the regolith securely in place, the crew used a thin stainless steel ram rod to push the keeper down into the drive tubes, and thus, compact and immobilize the regolith for transport and transit from the lunar surface to the curation facility at NASA JSC. 73002 was compacted a second time before it was transported to the UTCT facility for XCT scanning, by using the ram rod to push the keeper further into the drive tube. This was done to mitigate any potential loosening of the keeper that could have occurred over its 50+ years life span and to immobilize the regolith within the drive tube so that no stratigraphic information would be lost since it was known that some void space was present within the 73002 drive tube based on the medical X-ray images that were taken in 1973 (Figure 4). Tightening the keeper was carried out within the nitrogen atmosphere inside the curation gloveboxes. 73001 was not further compacted as the keeper was not deployed correctly on the lunar surface, and thus, the drive tube had to be transported and XCT scanned while situated within the CSVC. Both sample 73001 and 73002 were compacted one last time during the extrusion process. Using the original dataset produced by the XCT scan of the cores, the location of clasts within the drive tube at different depths was measured prior to the extrusion process and then compared to the location of the clasts after the extrusion process by measuring their location within the dissected intervals. To do so, the distance of the center of each clast was measured in relation to the top and bottom of the drive tube. Figure 18 shows the relative displacement of the clasts within 73002; Figure 19 shows the relative displacement of clasts within 73001. For both cores, most of the compaction seems to have occurred around larger clasts and in the direction of the extrusion (bottom of core towards top of the core); however, a less strong and opposite directed compaction force seemed to also have taken place during the extrusion process at the top of the drive tube, most likely caused by friction between the regolith, the follower clam from the extrusion apparatus, and the receptacle onto which the core was extruded (Figure 18,19). Furthermore, 73002 was compacted more compared to 73001 as apparent by the greater relative displacement of clasts within that core.

4.5 Sampling depth of the double drive tube

Images from the lunar surface show that double drive tube sample 73001/2 was fully hammered into the lunar surface at Station 3 of Apollo 17 landing site, and therefore sampled lunar regolith to a depth of 70.6 cm into the South Massif landslide area known as the “light mantle deposit” in the Taurus Littrow Valley (Wolfe et al., 1981). Due to complications during the separation of the upper (73002) and lower (73001) portions of the drive tube, not the entire 70.6 cm regolith column made it back to Earth. Although 73002 was originally full, and thus, sampled from 0-35 cm deep within the lunar regolith, astronaut Cernan saw material fall out of the drive tube before the Teflon containment cap could be put on the bottom of 73002. He observed that 73002 was only about 2/3 full based on how far the ramrod was able push the “keeper” down into the drive tube to immobilize the core for transport. This 2/3 estimate was confirmed by medical X-ray scans during the PE of 73002, which showed there to be ~23.5 cm of material in the 73002 core, which included considerable observed void space (Butler et al 1973). Thus, the material in the 73002 core likely represents a depth interval from 0 cm extending down to 20-23 cm depth, meaning that 12-15 cm of material was lost out of the 73002 drive tube bottom on the lunar surface. 73001, the bottom half of the double drive tube, came home completely full, and thus likely contains material from 35-70 cm beneath the lunar surface. These observations are consistent with various geochemical and isotopic data sets (see Sun et al., 2021a,b; Shearer et al., 2022, 2024).

5 Lessons learned from ANGSA that feed forward to Artemis.

Returning to the Moon with Artemis to collect and return lunar samples from a different region than Apollo, will enable discoveries of processes thus far unknown and enable a slew of new science including the opportunity to test hypotheses. Sample curation will play a critical part in all the different stages of the Artemis missions to return these valuable samples safely, ensuring their integrity, and thus maximizing their scientific return for centuries to come. The lessons learned from PE of ANGSA samples as well as recently returned samples from other bodies such as Bennu (OSIRIS-REx) can be directly applied to Artemis. Below are some of the valuable lessons learned from ANGSA that can be directly applied to PE for Artemis III:

(1) Extensive practice with mock-up gloveboxes as well as analog samples contained in flight-like hardware is crucial for successful sample processing. This practice will normalize the movements and motions required during sample handling and minimize the risk of sample integrity loss, and subsequent science loss, and therefore facilitate nominal processing of returned samples. Practice includes building and operating curation equipment, interfacing of geology sample containers with existing curation equipment, and communication with other processors and curators during PE.

(2) Having flight spares of geology sample containers and/or access to structural drawings of the hardware so that they can be duplicated with less expensive 3-D printed mockups are crucial for practice, interfacing with existing curation equipment and for determining the correct order of operations during PE that will minimize risk and mitigate any loss of sample integrity.

(3) More than four hours per day in the lab doing PE is not sustainable for any individual and will introduce mistakes that could lead to science loss due to the increased mental and cognitive workload under stress in a cleanroom environment. Furthermore, meticulous

documentation must be part of PE and curation, including documenting the environment that each sample will see at any given point (e.g., during transfer). Adequate time needs to be allotted to update the data records for each sample, enter information into internal databases, annotate images, transcribe notes and sketches, etc. The amount of time needed for documentation and database upkeep outside the cleanroom is about equal to the amount of time needed inside the cleanroom for a given sample-processing task.

(4) Multiple trained curation personnel are needed in the clean room during PE to work on important processing and documentation tasks. Redundancy will minimize human error and maximize PE time (e.g., illegible handwriting, transposed numbers, etc.)

(5) Science team participation during PE is extremely valuable for the science team as it highlights steps during PE and serves as a learning experience for those who don't work within curation daily. However, ANGSA demonstrated that training new science team members on a weekly or every-other-week time schedule (pre-pandemic) will slow the PE process down by 40%, posing a risk to any time-sensitive measurements that rely on rapid processing and allocation and posing a risk to producing the PE catalog within the required amount of time. Reducing training times by establishing a small, pre-designated PE team that could be integrated with curation prior to sample return, could be part of the pre-return practice exercises, and who can stay for the designated time under which PE is to be carried out could circumvent these risks.

(6) Dissecting individual core samples takes 6-8 months at a minimum. Dissection during hurricane season could disrupt the process and can affect sample integrity if not handled carefully. Preliminary Examination for most sample return missions is a period of 6 months after which the initial sample catalog is released. These timelines require that core dissection is not part of PE, instead it is a process that will occur during the extended examination phase. Consequently, the initial sample catalogs for Artemis will include undissected core samples that will not likely be available for request until after they are dissected and added to the sample catalog during extended examination.

(7) To carry out non-routine specialized measurements (such as gas extraction) in a timely manner, instrument and laboratory developments need to take place and be tested and

validated prior to sample return, and thus funding needs to be distributed sufficiently early to accommodate these timelines.

(8) Taking extra measures to clean the airlock after every third use, using extra protection (e.g., smock over bunny suit, and extra nitril gloves), proved to minimize organic and microbial contamination. Tests carried out before ANGSA started showed that cleaning the airlock more often didn't minimize contamination levels any further than after every third use, but cleaning it less often than every third use increased the risk of contamination. Furthermore, the airlock and sample processing environment should be monitored for inorganic, organic, and biological contamination on a regular basis.

(9) The use of X-ray computed tomography (XCT) has proven invaluable before and during the processing and preliminary examination of ANGSA samples 73001 and 73002. XCT scanning not only provides (I) a permanent record of the stratigraphy prior to extrusion, it also provides (II) the sample processors with information about potential pitfalls (e.g., void spaces, fractures, etc.) that they might encounter during the extrusion and dissection process, and thus, lowering the mental and cognitive workload by reducing stress of the unknown; and (III) it adds context for dust-coated rock fragments without compromising their sample integrity.

(10) The initial scans of the bottom and the top of the drive tubes (especially those within sealed containers) are critical in the assessment of tool usages (e.g., piercing tool, keeper), and thus the successful piercing, gas extraction, whole-core scanning, and extrusion.

(11) Multispectral imaging is a non-destructive, contamination-free technique for pristine samples if the measurements are carried out exterior to the glovebox through a glass top or observation port. Multispectral imaging can represent a quick and convenient tool for preliminary examination of soils to assess the degree of space weathering and obtain compositional information (i.e., FeO, TiO_2). However, while this information can provide important guidance for sample dissection, allocation, and distributions, the line between sample science that should be carried out by sample PIs and basic characterization of the sample for the initial PE catalog is not always clear and must be defined in an approved sample curation plan as outlined in NASA Procedural Requirement (NPR) 7100.5.

For decades Apollo has loomed large over new members of the lunar science community. Once again, the lessons of Apollo inform a new generation, and that new generation is now better prepared for the upcoming era of lunar surface exploration.

Acknowledgements:

The information in this paper represents just a portion of the overall ANGSA program effort. While there are too many people to list everyone by name, we'd like to draw special attention to a few. We'd like to thank the other 8 science PIs whose teams came together to make the overall project such a success: Jessica Barnes, Kate Burgess, Barbara Cohen and Natalie Curran, Darby Dyar, Jamie Elsila, Jeff Gillis-Davis, Alex Sehlke, and Kees Welton. Many members of the science team came into the lab to aid with the PE process including: Cari Corrigan, Barbara Cohen, Francesca McDonald, Jessica Barnes, Zoë Wilbur, Michelle Thompson, James McFadden, Kun Wang, Natalie Curran, Michael Cato, and Chris Yen. A special thanks is needed for Judy Allton and her tireless efforts as we prepared to open the first core in >25 years, as well as the many clean-room technicians and electromechanical technicians within the curation office who enabled our work by keeping our equipment and labs clean and in working order. Finally, we'd also like to thank Jeff Grossman, Sarah Noble, and Kathleen Vander Kaaden from NASA Headquarters for the funding, organization, and oversight on the project over the past few years.

Data Availability Statement

The data for this work is presented in Tables and Figures in the manuscript. In addition, all the data can be found in form or excel sheets, image files, XCT videos, etc. are publicly available from the lunar curation website in the form of Appendix 1-6 at https://curator.jsc.nasa.gov/lunar/angsa_catalog.cfm.

References:

Allton, J.H. (1989). Catalog of Apollo lunar surface geological sampling tools and containers. *JSC-23454 pp 97; Curator's Office;* NASA Lyndon B. Johnson Space Center; https://curator.jsc.nasa.gov/lunar/catalogs/other/jsc23454toolcatalog.pdf.

Athiray, P.S., Narendranath, S., Sreekumar, P., et al. (2013). Validation of methodology to derive elemental abundances from X-ray observations on Chandrayaan-1. *Planetary Space Sci*. 75, 188–194. https://doi.org/10.1016/j.pss.2012.10.003.

Benna, M., Hurley, D.M., Stubbs, T.J., Mahaffy, P.R., Elphic, R.C. (2019). Lunar soil hydration constrained by exospheric water liberated by meteoric impacts. *Nat Geosci* 12:333–338

Butler, P. (1973). Lunar sample information catalog, Apollo 17. MSC 03211; NASA Lyndon B. Johnson Space Center; *https://curator.jsc.nasa.gov/lunar/lsc/73001.pdf*.

Cain, J.R. (2010). Lunar dust: the hazard and astronaut exposure risks. *Earth, Moon, and Planets*, 107(1), 107-125.

Charette, M.P., McCord, T.B., Pieters, C. and Adams, J.B. (1974). Application of remote spectral reflectance measurements to lunar geology classification and determination of titanium content of lunar soils. *Journal of Geophysical Research*, 79(11), pp.1605-1613.

Crawford, I.A. and Joy, K.H. (2014). Lunar exploration: opening a window into the history and evolution of the inner Solar System. *Philosophical Transactions of the Royal Society A: Mathematical, Physical and Engineering Sciences*, 372(2024), p.20130315.

Crawford, I.A., Fagents, S.A., Joy, K.H. and Rumpf, M.E. (2010). Lunar palaeoregolith deposits as recorders of the galactic environment of the Solar System and implications for astrobiology. *Earth, Moon, and Planets*, 107, pp.75-85.

Crawford, I.A., Joy, K.H., Pasckert, J.H. and Hiesinger, H. (2021). The lunar surface as a recorder of astrophysical processes. *Philosophical Transactions of the Royal Society* A, 379(2188), p.20190562.

Dartois, E., Kebukawa, Y., Yabuta, H., Mathurin, J., Engrand, C., Duprat, J., Bejach, L., Dazzi, A., Deniset-Besseau, A., Bonal, L. and Quirico, E. (2023). Chemical composition of carbonaceous asteroid Ryugu from synchrotron spectroscopy in the mid-to far-infrared of Hayabusa2-returned samples. *Astronomy & Astrophysics*, 671, p.A2.

Day, J.M.D., Floss, C., Taylor, L.A., Anand, M., Patchen, A.D. (2006). Evolved mare basalt magmatism, high Mg/Fe feldspathic crust, chondritic impactors, and the petrogenesis of Antarctic lunar breccia meteorites Meteorite Hills 01210 and Pecora Escarpment 02007. *Geochim Cosmochim Acta* 70:5957–5989

Delano, J.W. (1991). Geochemical comparison of impact glasses from lunar meteorites ALHA81005 and MAC88105 and Apollo 16 regolith 64001. *Geochim Cosmochim Acta* 55:3019–3029

Demidova, S.I., and Badyukov, D.D. (2023). Peculiarities of the Extraterrestrial Basalts of the Solar System with Reference to the Exoplanet Science: a Brief Review. *Geochemistry International* 61.5 (2023): 453-467.

Donaldson Hanna, K.L., Greenhagen, B.T., Patterson III, W.R., Pieters, C.M., Mustard, J.F., Bowles, N.E., Paige, D.A., Glotch, T.D. and Thompson, C. (2017). Effects of varying environmental conditions on emissivity spectra of bulk lunar soils: Application to Diviner thermal infrared observations of the Moon. *Icarus*, 283, pp.326-342.

Eckley, S.A., Zeigler, R.A., Ketchum, R.A., Edey, D., Hanna, R.D., Gross, J., O'Neal, E., McCubbin, F.M., Shearer, C.K., and the ANGSA Science Team (this volume; in review). Characterization of Apollo Drive Tube Samples 73001 and 73002 by X-ray Computed Tomography. *Journal of Geophysical Research: Planets, Special ANGSA volume*, in review.

Elardo, S.M., Pieters, C.M., Dhingra, D., Donaldson Hanna, K.L., Glotch, T.D., Greenhagen, B.T., Gross, J., Head, J.W., Jolliff, B.L., Klima, R.L., Magna, T., McCubbin, F.M., Ohtake, M. (2023). The evolution of the lunar crust. *Rev Mineral Geochem* 89:293–338

Elphic, R.C., Lawrence, D.J., Feldman, W.C., et al. (1998). Lunar Fe and Ti abundances: comparison of lunar prospector and Clementine data. *Science* 281 (5382), 1493–1496. https://doi.org/10.1126/science.281.5382.1493.

Elphic, R.C., Lawrence, D.J., Feldman, W.C., et al. (2000). Lunar rare earth element distribution and ramifications for FeO and TiO_2: lunar prospector neutron spectrometer observations. *J. Geophys. Res.: Planets 105* (E8), 20333–20345. https://doi.org/10.1029/1999je001176.

Elphic, R.C., Lawrence, D.J., Feldman, W.C., et al. (2002). Lunar prospector neutron spectrometer constraints on TiO2. *J. Geophys. Res.: Planets* 107 (E4). https://doi.org/10.1029/2000je001460, 8–1.

Elsila, J.E., Aponte, J.C., Dworkin, J.P., Glavin, D.P., McLain, H.L., Simkus, D.N. and ANGSA Science Team (2022a). Trace Levels of Volatile Organic Compounds and Cyanide in the Apollo 73002 Core Sample. In *Lunar and Planetary Science Conference* no.53; p. 1212.

Elsila, J.E., Aponte, J.C., Dworkin, J.P., Glavin, D.P., McLain, H.L., Simkus, D.N. and ANGSA Science Team (2022b). Organic Compounds and Cyanide in the Apollo 17 ANGSA Samples. In *Apollo 17-ANGSA Workshop* (Vol. 2704, p. 2015).

Elsila, J.E., Callahan, M.P., Dworkin, J.P., Glavin, D.P., McLain, H.L., Noble, S.K. and Gibson Jr, E.K. (2016). The origin of amino acids in lunar regolith samples. *Geochimica et Cosmochimica Acta*, 172, pp.357-369.

Elsila, J.E., Aponte, J.C., McLain, H.L., Simkus, D.N., Dworkin, J.P., Glavin, D.P., Zeigler, R.A., McCubbin, F.M. and ANGSA Science Team (2024). Soluble organic compounds and cyanide in Apollo 17 lunar samples: Origins and curation effects. *Journal of Geophysical Research: Planets*, 129(4), p.e2023JE008133.

Eugster, O., Eberhardt, P., Geiss, J., Grögler, N., Jungck, M., Meier, F., Mörgeli, M., Niederer, F. (1984). Cosmic ray exposure histories of Apollo 14, Apollo 15, and Apollo 16 rocks. *Proc Lunar Planet Sci Conf* 14:498–512

Fagan, A.L., Neal, C.R., Simonetti, A., Donohue, P.H., & O'Sullivan, K.M. (2013). Distinguishing between Apollo 14 impact melt and pristine mare basalt samples by geochemical and textural analyses of olivine. *Geochimica et Cosmochimica Acta*, 106, 429-445.

Feist, B., Slater, S., and Bennet, C. (2016) Apollo in real time: Apollo 17; *https://apolloinrealtime.org/17*.

Feldman, W.C., Barraclough, B.L., Maurice, S., et al. (1998). Major compositional units of the moon: lunar prospector thermal and fast neutrons. *Science* 281 (5382),1489–1493. https://doi.org/10.1126/science.281.5382.1489.

Feldman, W.C., Lawrence, D.J., Elphic, R.C., et al. (2000). Chemical information content of lunar thermal and epithermal neutrons. *J. Geophys. Res.: Planets* 105 (E8), 20347–20363. https://doi.org/10.1029/1999je001183.

Fu, X., Yin, C., Jolliff, B.L., Zhang, J., Chen, J., Ling, Z., Zhang, F., Liu, Y. and Zou, Y. (2022). Understanding the mineralogy and geochemistry of Chang'E-5 soil and implications for its geological significances. *Icarus*, 388, p.115254.

Gaddis, L.R., Joy, K.H., Bussey, B.J., Carpenter, J.D., Crawford, I.A., Elphic, R.C., Halekas, J.S., Lawrence, S.J., Xiao, L. (2023). Recent exploration of the Moon: Science from lunar missions since 2006. *Rev Mineral Geochem* 89:1–51.

Gaffney, A.M., Borg, L.E., Depaolo, D.J., Irving, A.J. (2008). Age and isotope systematics of Northwest Africa 4898, a new type of highly depleted mare basalt. *Lunar Planet Sci* 34:#1877

Gaffney, A.M., Gross, J., Borg, L.E., Donaldson Hanna, K.L., Draper, D.S., Dygert, N., Elkins-Tanton, L.T., Prissel, K.B., Prissel, T.B., Steenstra, E.S., van Westrenen, W. (2023). Magmatic evolution I: Initial differentiation of the Moon. *Rev Mineral Geochem* 89:103–145

Grande, M., Browninga, R., Waltham, N., et al. (2001). The D-CIXS X-ray mapping spectrometer on SMART-1[J]. *Planet. Space Science* 51 (6), 427–433. https://doi.org/ 10.1007/978-94-010-0800-6 15.

Green, R.O., Pieters, C., Mouroulis, P., Eastwood, M., Boardman, J., Glavich, T., Isaacson, P., Annadurai, M., Besse, S., Barr, D. and Buratti, B. (2011). The Moon Mineralogy Mapper (M3) imaging spectrometer for lunar science: Instrument description, calibration, on-orbit measurements, science data calibration and on-orbit validation. *Journal of Geophysical Research: Planets*, 116(E10).

Gross, J., Joy, K.H. (2016). Evolution, lunar: From magma ocean to crust formation. In: *Encyclopedia of Lunar Science.* Cudnik B (Ed) Springer International Publishing

Gross, J., Treiman, A.H., Mercer, C.N. (2014). Lunar feldspathic meteorites: constraints on the geology of the lunar highlands, and the origin of the lunar crust. *Earth Planet Sci Lett* 388:31–328

Gross, J., Hilton, A., Prissel, T.C., Setera, J.B., Korotev, R.L., Calzada-Diaz, A. (2020). Geochemistry and petrogenesis of Northwest Africa 10401: a new type of the Mg-Suite Rocks. *J Geophys: Planets* 125:1–24

Gross, J., Krysher, C., Mosie, A., Zeigler, R.A., McCubbin, F.M. and Shearer, C. (2021) Preliminary Examination Process of Apollo Core 73002-Insights and Lessons Learned From ANGSA for Future Sample Return Missions. In *Lunar and Planetary Science Conference* 52; p. 2684.

Gross, J., Mosie, A., Krysher, C., Eckley, S.A., Zeigler, R.A., McCubbin, F.M., Shearer, C.K. and Angsa Science Team (2022) Processing Apollo Core Sample 73001/2—Insights from ANGSA to Prepare for Future Sample Return Missions to the Moon and Beyond. In *Apollo 17-ANGSA Workshop* (Vol. 2704, p. 2012).

Hallis, L.J., Anand, M., Greenwood, R.C., Miller, M.F., Franchi, I.A., and Russell, S.S. (2010). The oxygen isotope composition, petrology and geochemistry of mare basalts: evidence for large-scale compositional variation in the lunar mantle. *Geochimica et Cosmochimica Acta*, 74(23), 6885-6899.

He, Q., Li, Y., Baziotis, I., Qian, Y., Xiao, L., Wang, Z., Zhang, W., Luo, B., Neal, C.R., Day, J.M. and Pan, F. (2022). Detailed petrogenesis of the unsampled Oceanus Procellarum: The case of the Chang'e-5 mare basalts. *Icarus*, 383, p.115082.4

Head, III J.W., Wilson, L., Hiesinger, H., van der Bogert, C., Chen, Y., Dickson, J.L., Gaddis, L.R., Haruyama, J., Jawin, E.R., Jozwiak, L.M., Li, C., Liu, J., Morota, T., Needham, D.H., Ostrach, L.R., Pieters, C.M., Prissel, T.C., Qian, Y., Qiao, L., Rutherford, M.R., Scott, D.R., Whitten, J.L., Xiao, L., Zhang, F., Ziyuan, O. (2023). Lunar mare basaltic volcanism: Volcanic features and emplacement processes. *Rev Mineral Geochem* 89:453–507

Hiesinger, H., Jaumann, R., Neukam, G., Head, J.W. (2000). Ages of mare basalts on the lunar nearside. *J Geophys Res* 105:29239–29276

Hiesinger, H., Head, J.W., Wolf, U., Jaumann, R., Neukum, G. (2003). Ages and stratigraphy of mare basalts in Oceanus Procellarum, Mare Nubium, Mare Cognitum, and Mare Insularum. *J Geophys Res* 108(E7):5065

Hiesinger, H., Head, J.W. III, Wolf, U., Jaumann, R., Neukum, G. (2010). Ages and stratigraphy of lunar mare basalts in Mare Frigoris and other nearside maria based on crater size–frequency distribution measurements. *J Geophys Res* 115:E03003

Hiesinger, H., Head, III J.W., Wolf, U., Jaumann, R., Neukum, G. (2011). Ages and stratigraphy of lunar mare basalts: A synthesis. *Geol Soc Am Spec Pap* 477:1–51

Hiesinger, H., van der Bogert, C.H., Pasckert, J.H., Funcke, L., Giacomini, L., Ostrach. L,R., Robinson, M.S. (2012). How old are young lunar craters? *J Geophys Res* (Planets) 117:E00H10

Hiesinger, H., van der Bogert, C.H., Michael, G., Schmedemann, N., Iqbal, W., Robbins, S.J., Ivanov, B., Williams, J.-P., Zanetti, M., Plescia, J., Ostrach, L.R., Head, III J.W. (2023). The lunar cratering chronology. *Rev Mineral Geochem* 89:401–451

Ito, M., Tomioka, N., Uesugi, M., Yamaguchi, A., Shirai, N., Ohigashi, T., Liu, M.C., Greenwood, R., Kimura, M., Imae, N. and Uesugi, K., (2022). Hayabusa2 returned samples: a unique and pristine record of outer Solar System materials from asteroid Ryugu.

James, J.T., and Kahn-Mayberry, N. (2009). Risk of adverse health effects from lunar dust exposure. *The human research program evidence book*, 317-330.

Jones, B.M., Aleksandrov, A., Dyar, M.D., Hibbitts, C.A., Orlando, T.M. (2020). Investigation of water interactions with Apollo lunar regolith grains. *JGR planets* 125, e2019JE006147; https://doi.org/10.1029/2019JE006147.

Joy, K.H., Zolensky, M.E., Nagashima, K. Huss, G.R., Ross, D.K., McKay, D.S., Kring, D.A. (2012). Direct detection of projectile relics from the end of the lunar basin–forming epoch. *Science* 336:1426–1429

Joy, K.H., Crawford, I.A., Curran, N.M., Zolensky, M.E., Fagan, A.F., Kring, D.A. (2016). The Moon: An archive of small body migration in the solar system. *Earth Moon Planets* 118:133–158.

Joy, K.H., Tartèse, R., Messenger, S., Zolensky, M.E., Marrocchi, Y., Frank, D.R., Kring, D.A. (2020). The isotopic composition of volatiles in the unique Bench Crater carbonaceous chondrite impactor found in the Apollo 12 regolith. *Earth Planet Sci Lett* 540:116265

Joy, K.H., Gross, J., Korotev, R.L., Zeigler, R.A., McCubbin, F.M., Snape, J.F., Curran, N.M., Pernet-Fisher, J.F. and Arai, T. (2023). Lunar meteorites. *Reviews in Mineralogy and Geochemistry*, 89(1), pp.509-562.

Ketcham, R.A., Hanna, R.D., Edey, D.R., Zeigler, R.A. and Eckley, S.A. (2022). Acquisition and Processing of X-Ray CT Whole-Core Data for Apollo Samples 73001 and 73002. *Apollo 17-ANGSA Workshop*, Vol. 2704, p. 2044.

Khan-Mayberry, N. (2008). The lunar environment: Determining the health effects of exposure to moon dusts. *Acta Astronautica*, 63(7-10), 1006-1014.

Kiefer, W.S., Macke, R.J., Britt, D.T., Irving, A.J. and Consolmagno, G.J. (2014). The density and porosity of lunar impact breccias and impact melt rocks and implications for GRAIL gravity modeling of the Orientale impact basin structure. *Geophys. Res. Lett*, 41, pp.5771-5777.

Krysher, C.H., Mosie, A.B., Gross, J., Zeigler, R.A., McCubbin, F.M. and Allton, J.H. (2020). Adventures in Lunar Core Processing: Timeline of and Preparation for Opening of Core Sample 73002 for the ANGSA Program. In *Lunar and Planetary Science Conference* 51, p. 2989 (No. JSC-E-DAA-TN77641).

Laul, J.C., Smith, M.R. and Schmitt, R.A. (1983). ALHA 81005 meteorite: Chemical evidence for lunar highland origin. *Geophysical Research Letters*, 10(9), pp.825-828.

Lawrence, D.J., Feldman, W.C., Barraclough, B.L., et al. (1998). Global elemental maps of the moon: the lunar prospector gamma-ray spectrometer. *Science* 281 (5382), 1484–1489. https://doi.org/10.1126/science.281.5382.1484.

Lawrence, D.J., Feldman, W.C., Barraclough, B.L., et al. (1999). High resolution measurements of absolute thorium abundances on the lunar surface. *Geophys. Res. Lett*. 26 (17), 2681–2684. https://doi.org/10.1029/1999gl008361.

Lawrence, D.J., Feldman, W.C., Barraclough, B.L., et al. (2000). Thorium abundances on the lunar surface. *J. Geophys. Res.: Planets* 105 (E8), 20307–20331. https://doi.org/10.1029/1999JE001177.

Lentfort, S., Bischoff, A., Ebert, S., & Patzek, M. (2021). Classification of CM chondrite breccias—Implications for the evaluation of samples from the OSIRIS-REx and Hayabusa 2 missions. *Meteoritics & Planetary Science*, 56(1), 127-147.

Liu, J., Sharp, M., Ash, D., Kring, D.A., Walker, R.J. (2015). Diverse impactors in Apollo 15 and 16 impact melt rocks: Evidence from osmium isotopes and highly siderophile elements. *Geochim Cosmochim Acta* 155:122–153

Lucey, P.G., Blewett, D.T., Hawke, B.R. (1998). Mapping the FeO and TiO2 content of the lunar surface with multispectral imagery. *J. Geophys. Res.: Planets* 103 (E2),3679–3699. https://doi.org/10.1029/97je03019.

Lucey, P.G., Blewett, D.T., Jolliff, B.L., (2000a). Lunar iron and titanium abundance algorithms based on final processing of Clementine ultraviolet-visible images. *J. Geophys. Res.: Planets* 105 (E8), 20297–20305. https://doi.org/10.1029/1999je001117.

Lucey, P.G., Taylor, G.J., Malaret, E. (1995). Abundance and distribution of iron on the moon. *Science* 268 (5214), 1150–1153. https://doi.org/10.1126/science.268.5214.1150.

Lucey, P.G., Blewett, D.T., Taylor, G.J., Hawke, B.R. (2000b). Imaging of lunar surface maturity. *J Geophys Res: Planets* 105:20377–20386

Lucey, P., Greenhagen, B., Hanna, K.D., Bowles, N., Flom, A., Paige, D. (2021). Christiansen feature map from the lunar reconnaissance orbiter diviner lunar radiometer experiment: improved corrections and derived mineralogy. *J. Geophys. Res.* https://doi.org/10.1029/2020JE006777.

Lucey, P.G., Greenhagen, B.T., Song, E., et al. (2017). Space weathering effects in Diviner Lunar Radiometer multispectral infrared measurements of the lunar Christiansen Feature: Characteristics and mitigation. *Icarus* 343–351. https://doi.org/10.1016/j.icarus.2016.05.010.

Lucey, P., Korotev, R.L., Gillis, J.J., et al. (2006). Understanding the lunar surface and space-moon interactions. *Rev. Mineral. Geochem*. 60 (1), 83–219. https://doi.org/10.2138/rmg.2006.60.2.

Lucey, P.G., Sun, L., Flom, A.J., Chertok, M.A., Zeigler, R.A., Gross, J., Shearer C.K. and Angsa Science Team (2023). Infrared Spectroscopy of Apollo 17 Core 73001: Implications for Lunar Surface Water. *Lunar and Planetary Science Conference*, 54; LPI Contributions, 2806, 1591.

McCubbin, F.M., Herd, C.D., Yada, T., Hutzler, A., Calaway, M.J., Allton, J.H., Corrigan, C.M., Fries, M.D., Harrington, A.D., McCoy, T.J. and Mitchell, J.L. (2019). Advanced curation of astromaterials for planetary science. *Space Science Reviews,* 215, pp.1-81.

McDonald, F., Schild, T., Bamsey, N., Apolloni, M., Biella, R., Butenko, Y., Dowson, A., Eckley, S., Gross, J., Jolliff, B. and Lindner, R. (2022). A unique lunar gas extraction event as part of the ANGSA Program and the lessons learned for a new generation of sample return missions. *Copernicus Meetings* No. EPSC2022-1117.

McIntosh, E.C., Day, J.M.D., Liu, Y., Jiskoot, C. (2020). Examining the compositions of impactors striking the Moon using Apollo impact melt coats and anorthositic regolith breccia meteorites. *Geochim Cosmochim Acta* 274:192–210

McLain, J.L., Loeffler, M.J., Farrell, W.M., Honniball, C.I., Keller, J.W. and Hudson, R. (2021). Hydroxylation of Apollo 17 soil sample 78421 by solar wind protons. *Journal of Geophysical Research: Planets,* 126(5), p.e2021JE006845.

Naito, M., Hasebe, N., Nagaoka, H., et al. (2018). Iron distribution of the moon observed by the Kaguya gamma-ray spectrometer: geological implications for the south pole Aitken basin, the Orientale basin, and the Tycho crater. *Icarus* 310, 21–31. https://doi.org/10.1016/j.icarus.2017.12.005.

Neal, C.R., Gaddis, L.R., Jolliff, B.L., Lawrence, S.J., Mackwell, S.J., Shearer, C.K., Valencia, S.N. (2023). New Views if the Moon 2. Reviews in Mineralogy and Geochemistry, Vol. 89. Series editor: Ian P. Swainson; Mineralogical Society of America, Geochemical Society. IS-SSN 1529-6466.

Nichols Jr, R.H., Hohenberg, C.M. and Olinger, C.T. (1994). Implanted solar helium, neon, and argon in individual lunar ilmenite grains: Surface effects and a temporal variation in the solar wind composition. *Geochimica et cosmochimica acta*, 58(2), pp.1031-1042.

Nyquist, L.E., Bogard, D.D., Shih, C.-Y. (2001). Radiometric chronology of the Moon and Mars. In: The Century of Space Science. Springer, Dordrecht, p 1325–1376

Parai, R., Rodriguez, J., Patzkowsky, S., Solari, N., Woody, K.A., Meshik, A., Pravdivtseva, O., Jolliff, B.L., Shearer, C.K., Sharp, Z.D. and Cassata, W. (2022). Noble Gas Isotopes in the Apollo 17 73001 Core Sample Vacuum Container Gas. In *Apollo 17-ANGSA Workshop* (Vol. 2704, p. 2028).

Pernet-Fisher, J., McDonald, F. E., Zeigler, R. A., and Joy, K. (2019). 50 years on: legacies of the Apollo programme. *Astronomy and Geophysics*, 60(4), 4.22-4.28. https://doi.org/10.1093/astrogeo/atz163

Prettyman, T.H., Hagerty, J.J., Elphic, R.C., et al. (2006). Elemental composition of the lunar surface: analysis of gamma ray spectroscopy data from lunar prospector. *J. Geophys. Res.: Planets* 111 (E12). https://doi.org/10.1029/2005je002656.

Qian, Y., Xiao, L., Wang, Q., Head, J.W., Yang, R., Kang, Y., van der Bogert, C.H., Hiesinger, H., Lai, X., Wang, G. and Pang, Y. (2021). China's Chang'E-5 landing site: Geology, stratig-raphy, and provenance of materials. *Earth and Planetary Science Letters*, 561, p.116855.

Regberg, A.B., Amick, C.L., Davis, R.E., Lewis, E.K., Mazhari, F., Mitchell, J.L., Owens, D.L. and McCubbin, F.M. (2021). A Method to Reduce Bioburden in Astromaterials Curation Facilities Without Introducing Unwanted Contamination. In *52nd Lunar and Planetary Science Conference*: p. 2491

Rezaie-Serej, S. and Outlaw, R.A. (1994). Thermal desorption of CO and H2 from degassed 304 and 347 stainless steel. *Journal of Vacuum Science & Technology A: Vacuum, Surfaces, and Films*, 12(5), pp.2814-2819.

Sato, H., Robinson, M.S., Lawrence, S.J., Denevi, B.W., Hapke, B., Jolliff, B.L. and Hiesinger, H. (2017). Lunar mare TiO2 abundances estimated from UV/Vis reflectance. *Icarus*, 296, pp.216-238.

Saxena, P., Killen, R. M., Airapetian, V., Petro, N. E., Curran, N. M., and Mandell, A. M. (2019). Was the Sun a slow rotator? Sodium and potassium constraints from the lunar regolith. The Astrophysical Journal Letters, 876(1), L16.

Schild, T., McDonald, F.E., de Medeiros, P., Apolloni, M., Bamsey, N., Biella, R., Butenko, Y., Dowson, A., Cowley, A., Lindner, R. and Makaya, A. (2022). Piercing Device for Gas Extraction from Apollo 17 Sample Container: Final Design and Key Learnings. In *Apollo 17-ANGSA Workshop* (Vol. 2704, p. 2013).

Schmitt, H.H., Petro, N.E., Wells, R.A., Robinson, M.S., Weiss, B.P., Mercer, C.M. (2017). Revisiting the field geology of Taurus-Littrow. *Icarus* 298:2–33.

Sharp, Z.D., Cano, E.J., Cato, M.J., Gargano, A.M., Shearer, C.K., and Ziegler, K.G. (2020). Hydrogen, Chlorine and Oxygen Isotope Analyses of the ANGSA Drivetube Samples. In *51st Annual Lunar and Planetary Science Conference*, no. 2326, p. 1286. 2020.

Sharp, Z.D., Shearer, C.K., Meshik, A., Parai, R., Pravdivtseva, O., Cassata, W., Gross, J., McCubbin, F., Zeigler, R., Jolliff, B.L. and McDonald, F. (2022). Major Element Gas Composition of the Apollo 73001 Inner (CSVC) and Outer Containers. In *Apollo 17-ANGSA Workshop* (Vol. 2704, p. 2052).

Shearer, C.K., Simon, S.B., Jolliff, B.L., McCubbin, F.M., Zeigler, R.A., Gross, J., Yen, C.K., Joy, K.H., Bell, S.K., Cato, M. and Eckley, S. (2022). A" New" Lunar Sample Return Mission Reveals a Fresh Perspective of Lunar Magmatism from Lithic Fragments from Double Drive Tube 73001/73002. In *Apollo 17-ANGSA Workshop* (Vol. 2704, p. 2003).

Shearer, C.K., McCubbin, F.M., Eckley, S., Simon, S.B., Meshik A., McDonald F., Schmitt H.H., Zeigler, R.A., Gross, J., Mitchell J., Krysher C., Morris R.V., Parai R., Jolliff, B.L., Gillis-Davis J.J., Joy K., Bell S.K., Lucey P., Sun L., Sharp Z., Dukes C., Sehlke A., Mosie A., Allton J., Amick C., Simon J., Erickson T.M., Barnes J.J., Dyar M., Burgess K., Petro N., Moriarty D., Curran N.M., Elsia J.E., Colina-Ruis R.A., Kroll T., Sokaras D., Isshii H.A., Bradley J.P., Sears D., Cohen B., Pravdiseva O., Thompson M.S., Neal C.R., Hana R., Ketchum R., Welton K., and the ANGSA science team (2024): Apollo Next Generation Sample Analysis (ANGSA): An Apollo Participating Scientist Program to Prepare the Lunar Sample Community for Artemis. *Space Science Reviews*, 220, 62; https://doi.org/10.1007/s11214-024-01094-x

Simon, S.B., Papike, J.J., & Laul, J.C. (1982). The lunar regolith-Comparative studies of the Apollo and Luna sites. Petrology of soils from Apollo 17, Luna 16, 20, and 24. In *Lunar and Planetary Science Conference, 12th, Proceedings. Section 1;* New York and Oxford, Pergamon Press, 1982, Vol. 12; p. 371-388.

Simon, S.B., Papike, J.J., & Shearer, C.K. (1984). Petrology of Apollo 11 regolith breccias. *Journal of Geophysical Research: Solid Earth*, 89(S01), C108-C132.

Simon, S.B., Papike, J.J., Shearer, C.K., and Laul, J.C. (1983). Petrology of the Apollo 11 highland component. *Journal of Geophysical Research: Solid Earth*, 88(S01), B103-B138.

Simpson, J.A. (1983) Introduction to the galactic cosmic radiation. In: *Shapiro MM (ed) Composition and Origin of Cosmic Rays*, Reidel, Amsterdam, p 1–24

Sun, L., Lucey, P.G., and Taylor, G.J. (2021a). Correlating Apollo soil mineralogical data with Kaguya spectral data for a global mineralogical classification. *Journal of Geophysical Research: Planets*, 126(5), e2020JE006445.

Sun, L., Lucey, P.G., Flom, A., Ferrari-Wong, C., Zeigler, R.A., Gross, J., Petro, N.E., Shearer, C.K., McCubbin, F.M., and The ANGSA Science Team (2021b). Multispectral Imaging and Hyperspectral Scanning of the First Dissection of Core 73002: Preliminary Results. Meteoritics & Planetary Science, 56, 1574-1584.

Swinyard, B.M., Joy, K.H., Kellett, B.J., Crawford, I.A., Grande, M., Howe, C.J., Fernandes, V.A., Gasnault, O., Lawrence, D.J., Russell, S.S., Wieczorek, M.A., Foing, B.H., the SMART-1 Team (2009). X-ray fluorescence observations of the moon by SMART-1/D-CIXS and the first detection of Ti Kα from the lunar surface. *Planet Space Sci* 57:744–750

Tachibana, S., Yurimoto, H., Nakamura, T., Noguchi, T., Okazaki, R., Yabuta, H., Naraoka, H., Sakamoto, K., Watanabe, S. and Tsuda, Y. (2022). Initial Analysis Activity of Hayabusa2-Returned Samples from C-Type Nearearth Asteroid (162173) Ryugu. *Meteoritics & Planetary Science*, 57, p6111.

Tikoo, S.M., Weiss, B.P., Buz, J., Lima, E.A., Shea, E.K., Melo, G., Grove, T.L. (2012). Magnetic fidelity of lunar samples and implications for an ancient core dynamo. *Earth Planet Sci Lett* 337–338:93–103

Tikoo, S.M., Weiss, B.P., Shuster, D.L., Suavet, C., Wang, H., Grove, T.L. (2017). A two-billion-year history for the lunar dynamo. *Sci Adv* 3:E1700207

Treiman, A.H. and Drake, M.J. (1983). Origin of lunar meteorite ALHA 81005: Clues from the presence of Terrae clasts and a very low-titanium mare basalt clast. *Geophysical Research Letters*, 10(9), pp.783-786.

Wagner, S. (2006). The Apollo experience lessons learned for constellation lunar dust management (No. JSC-CN-10841).

Welten, K.C., Caffee, M.W., Nishiizumi, K. and ANGSA Science Team (2022). Cosmogenic Radionuclides in Lunar Core 73002/01: Cosmic-Ray Exposure History and Regolith Mixing of the Lunar Surface. In *Apollo 17-ANGSA Workshop* (Vol. 2704, p. 2046).

Wieczorek, M.A., Neumann, G.A., Nimmo, F., Kiefer, W.S., Taylor, G.J., Melosh, H.J., Phillips, R.J., Solomon, S.C., Andrews-Hanna, J.C., Asmar, S.W., Konopliv, A.S. (2013). The crust of the Moon as seen by GRAIL. *Science* 339:671–675

Wieczorek, M.A., Weiss, B.P., Breuer, D., Cébron, D., Fuller, M., Garrick-Bethell, I., Gattacceca, J., Halekas, J.S., Hemingway, D.J., Hood, L.L., Laneuville, M., Nimmo, F., Oran, R., Purucker, M.E., Rückriemen, T., Soderlund, K.M., Tikoo, S.M. (2023). Lunar magnetism. *Rev Mineral Geochem* 89:207–241

Wieler, R. (2016). Do lunar and meteoritic archives record temporal variations in the composition of solar wind noble gases and nitrogen? A reassessment in the light of Genesis data. *Chemie der Erde* 76:463–480

Wolfe, E.W., Bailey, N.G., Lucchitta, B.K., Muehlberger, W.R., Scott, D.H., Sutton, R.L. and Wilshire, H.G. (1981). The Geologic Investigation of the Taurus-Littrow Valley: Apollo 17 Landing Site. *United States Goelogical Surv. Prof. Pap.* 1080.

Wood, J.A. (1975). Lunar petrogenesis in a well-stirred magma ocean. In: Lunar Science Conference, 6th, Houston, Tex., March 17-21, 1975, *Proceedings. Volume 1 (A78-46603 21-91) New York, Pergamon Press, Inc.*, 1975, p. 1087-1102.

Zeigler, R.A., Mosie, A.B., Corrigan, C., Costello, L.J., Kent, J.J., Krysher, C.H., Watts, L.A. and McCubbin, F.M. (2019). The Apollo sample collection: 50 years of solar system insight. *Elements*, 15(4), pp.286-287.

Zeigler, R.A., Eckley, S., Edey, D., Ketcham, R.A., Hanna, R.D., Gross, J., McCubbin, F.M. and Shearer, C.K. (2022). X-Ray Computed Tomography During Preliminary Examination of Apollo Drive Tube 73001. In *85th Annual Meeting of The Meteoritical Society*.

Zeigler, R.A., Eckley, S., Hanna, R.D., Edey, D., Ketcham, R.A, Gross, J., McCubbin, F.M. and the ANGSA Science Team (2021). Using X-Ray Computed Tomography to Image Apollo Drive Tube 73002. In *Lunar and Planetary Science Conference* No.52, p.2632

Zuber, M.T., Smith, D.E., Watkins, M.M., Asmar, S.W., Konopliv, A.S., Lemoine, F.G., Melosh, H.J., Neumann, G.A., Phillips, R.J., Solomon, S.C. (2013). Gravity field of the

Moon from the Gravity Recovery and Interior Laboratory (GRAIL) mission. *Science* 339:668–671.

Table 1: List of gas samples taken from sealed sample 73001.

Table 2: Classification of rock particles > 4 mm via XCT scanning.

Figure 1: a) Returned samples representing the ancient crust such as anorthosites (Apollo sample 60025); b) modified crust such as breccias (Apollo sample 67016) and impact melts; c) or additions made to the crust such as basalts (Apollo sample 10049) or exogenic materials. Images of rocks from the Apollo compendium (Meyer, 2012).

Figure 2: Apollo samples have anchored lunar science by calibrating instruments (a) and scientific data sets (b, c). In addition, mineral chemistry (d) and physical properties (c, e) are used to understand lunar evolution through space and time (f-h), and exogenic material found within samples provide insights into solar system climate and our place within the galaxy (g,h). See text for more details ([1]Meyer, 2012; [2]Lucey et al., 1995; [3]Hiesinger et al., 2023;[4] Kiefer et al., 2014; [5]Gross et al., 2014; [6] Tikoo et al., 2012, 2017; [7,8]Treiman and Drake, 1983; [7,8]Laul et al, 1983; [9]Joy et al., 2016).

Figure 3: Flowchart to distinguish between science investigations, basic characterization, preliminary examination, and extended examination (after McCubbin et al., 2019). Y = Yes; N = No; XCT = X-ray Computed Tomography; BC = Basic Characterization; PE = Preliminary Examination.

Figure 4: Comparison between the medical X-ray dataset from 1973 and XCT dataset from 2019. An unknown amount of material fell out the bottom of this upper drive tube during the securing process on the lunar surface, which manifested in a void space visible in the X-ray image taken in 1973 (white arrow).

Figure 5: a) Gas extraction manifold with the 73001 OVC attached. The water-ice bath, used to try to remove possible hydrocarbon gas contamination, was only used during OVC2 extraction. Drs. Gross and Pravdivtseva for scale; b) insertion process of the CSVC into the piercing tool:

(b1) the CSVC going into the piercing tool insert; (b2) the piercing tool insert being placed into the main body of the piercing tool, with the piercing tool top/chisel in the foreground; (b3) placing the piercing tool top/chisel on to the piercing tool main body. Drs. Gross and McDonald for scale; c) gas extraction manifold with the piercing tool (with the 73001 CSVC inside).

Figure 6: Current configuration of the Gas Extraction Manifold showing a) the additional stainless steel 2-liter bottle added to the system, as well as b) the two available conflate distribution ports for Principal Investigators (PIs) subsamples to be taken through.

Figure 7: a) Whole core XCT images of drive tubes 73001 and 73002 with representative cross-sectional slices shown for b) 73002 (slice 1748) and c) 73001 (slice 5446). This image is made from the 51.6 μm per voxel down-sampled data.

Figure 8: a) XCT cross section view of the top of the 73001 CSVC after the gas extraction was done. The stainless-steel keeper's (purple arrow) prongs (yellow arrows) are supposed to be holding the regolith material in place by grabbing on to the sides of the inner aluminum drive tube walls (light blue arrows). b) XCT cross section view of the bottom of the 73001 CSVC after the gas extraction. The stainless steel CSVC has clearly been pierced (orange arrow), and while the Teflon cap (dark yellow arrow) on the 73001 drive tube has been dented, it is still intact.

Figure 9: a) Lunar processor Andrea Mosie preparing to remove the 73001 drive tube from the CSVC; b) adding the end effectors to the drive tube to enable the extrusion; c) drive tube inside the extrusion apparatus and core being pushed onto the receptacle; d) extruded core with quartz top, on dissection table with happy extrusion team Andrea Mosie and Dr. Juliane Gross.

Figure 10: a) Sketch of 73001/2 core with locations of each pass. For pass 1, the quartz top (light gray) and the first plate (dark gray) was removed. Two more plates are re-moved for each subsequent pass. Each plate is 0.5 cm thick, thus removing 2 plates leaves the core stick out 1cm above the next plate level. TS (thin section) is the portion reserved for epoxy impregnation and encapsulation to make thin sections. b) De-rind process to expose the pristine core material by removing the outermost 1-2mm rind. The core is marked in 5 cm intervals, the plate is etched with a cm scale.

Figure 11: Pass 2 of 73002 core. a) The core sticks out above plate level for Pass 2 after removal of two table plates. b) The smooth sides of the core have been de-rinded to expose the pristine material underneath. The core is mid dissection of pass 2 in this image. Large clasts that protrude through multiple passes are kept in place and are dissected around (white arrow). These large clasts are removed from the core after pass 3 is dissected, prior to transferring the TS portion (Figure 10) to the Apollo thin section lab. c) Sieved and sorted >1 mm particles into their respective size fractions on the Teflon cap (left, scale is in cm); example of a triple bagged 4-10 mm particle (right) with a gloved finger in the background. The plate contains an etched cm scale.

Figure 12: Examples of the different data sets developed and collected during ANGSA and a schematic sketch on how they are all connected to each other. a) inventory spreadsheet; b) sketches and notes; c) XCT images and videos; d) photo particle data with multiple photo angles and labeled clasts, with a cm scale bar.

Figure 13: a) Example of the sketches taken in the lab during dissection and the cleaned up, b) digitized version that contains information about clast locations and core properties.

Figure 14: Continuous core section process steps. a) 73002 core impregnated with epoxy in the core dissection plate with a cm scale; b) 73002 core encased in its secondary encapsulation epoxy with a cm scale ruler; c) silicone secondary encapsulation mold and 73001 core in its secondary encapsulation epoxy, turned over to show the depth and fiducial markings as well as top and bottom tags embedded within the epoxy; d) the 4 potted butts produced from one half of the 73002 core after cutting b) in half lengthwise, which were used to produce 2 initial sets of continuous core thin sections. Scale in a)-c) is in cm; cube edge in d) is 1 inch.

Figure 15: Single slice XCT image views of 10 typical lithologies encountered of the 352 particles scanned that were > 4mm. a) high-Ti basalt, b) high-Ti basalt, c) recrystallized high-Ti basalt, d) low-Ti basalt, e) low-Ti basalt, f) agglutinate, g) regolith breccia, h) cataclastic anorthosite, i) regolith breccia dominated by black glass, j) anorthosite. Scale bars are 1 mm.

Figure 16: Lithology of all >4 mm clasts. a) Lithologies in 73002; b) lithologies in 73001.

Figure 17: a-d) Grainsize analyses for 73002 and for 73001 (e-h). Number of grains in all sieved passes (passes 1 & 2) for a) 73002 and e) 73001 compared to the mass of all material from all

sieved passes (b, f). c) XCT images of 73002 and g) of 73001 are shown to highlight the dissected and sieved material above the yellow line which represents the dissected surface of pass 2 for both cores. Photographs of the dissected surface of pass 2 for each respective core (d = 73002; h = 73001) with clasts sticking out that go into pass 3.

Figure 18: Relative displacement of clasts within 73002 drive tube during extrusion. The location of the clasts pre-extrusion was measured using the XCT data set of the core (a) and compared to the location of the clasts after the extrusion and dissection (c). The orange arrows in the relative displacement graph (b) indicate that the direction of compaction is stronger at the bottom of the core from the direction of extrusion and weaker at the top, most likely caused by friction between the regolith, the follower clam, and the receptacle.

Figure 19: Relative displacement of clasts within 73001 drive tube during extrusion. The location of the clasts pre-extrusion was measured using the XCT data set of the core (a) and compared to the location of the clasts after the extrusion and dissection (c). The orange arrows in the relative displacement graph (b) indicate that the direction of compaction is stronger at the bottom of the core from the direction of extrusion and weaker at the top, most likely caused by friction between the regolith, the follower clam, and the receptacle.

Figure 1.

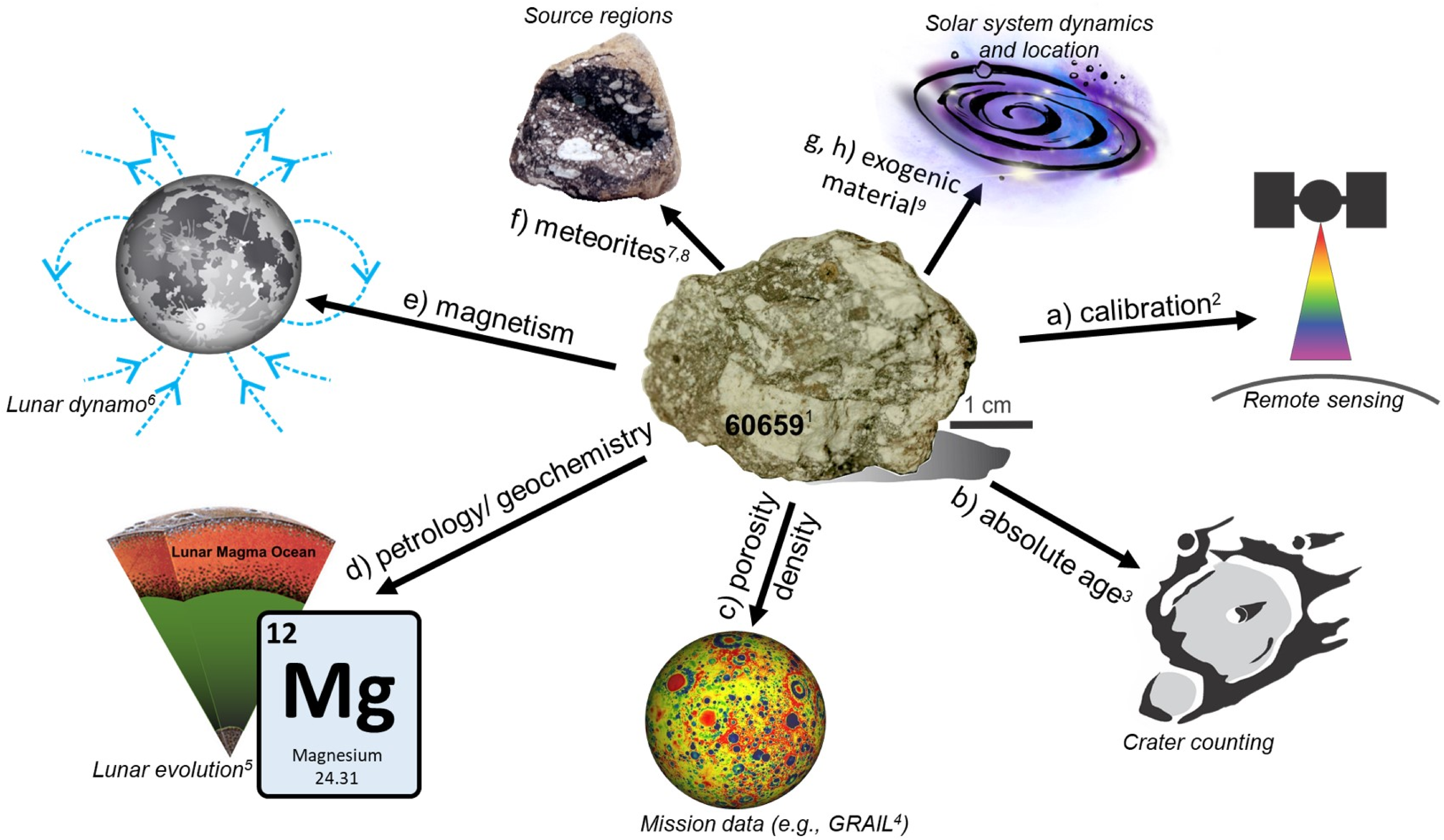

Source regions
Solar system dynamics and location
g, h) exogenic material[9]
f) meteorites[7,8]
e) magnetism
a) calibration[2]
Remote sensing
Lunar dynamo[6]
60659[1]
1 cm
d) petrology/ geochemistry
c) porosity
density
b) absolute age[3]
Lunar Magma Ocean
12
Mg
Magnesium
24.31
Lunar evolution[5]
Crater counting
Mission data (e.g., GRAIL[4])

Figure 2.


a)
60025
b)
67016
c)
10049,0

Figure 3.

Can results of the investigation lead to a stand-alone paper?
Y
N
Science (not PE or BC)
Can the investigation be done without altering or touching the samples
Y
Basic Characterization (BC)*
Exception
N
N
Are the results critical to create a meaningful sample catalog?
Y
Preliminary Examination (PE)#
Is it time sensitive science (within 6 months after return)?
Y
Conduct in parallel to PE
Y = Yes; N = No; PE = preliminary Examination; BC = basic characterization
*Basic Characterization (BC)
Documentation of sample containers & seals upon arrival via different methods (e.g., XCT, photos, videos, notes)
#Preliminary Examination (PE)
Documentation (e.g., photos, videos) of opened sample states (e.g., crumbled, broken, intact) and character (e.g., mass, size, texture).
Extended Examination
(carried out on small subset of samples during PE time permitting; carried out during long term curation)
Documentation of physical sample properties via different methods such as sieving, XCT scanning, thin-sectioning, grain mounts, grain size distribution, maturity, core dissection.

Figure 4.

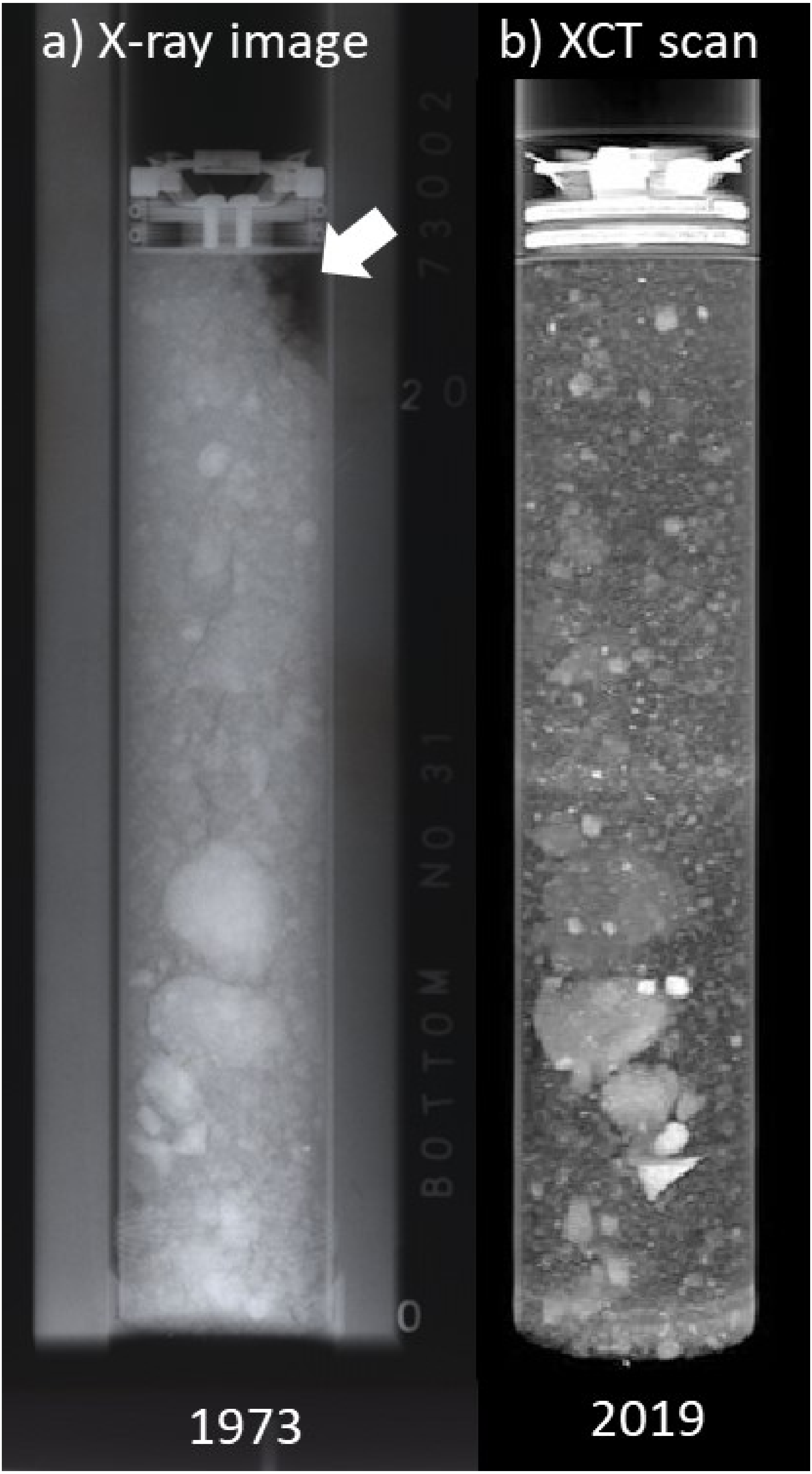
a) X-ray image
b) XCT scan
73002
20
BOTTOM NO 31
0
1973
2019

Figure 5.

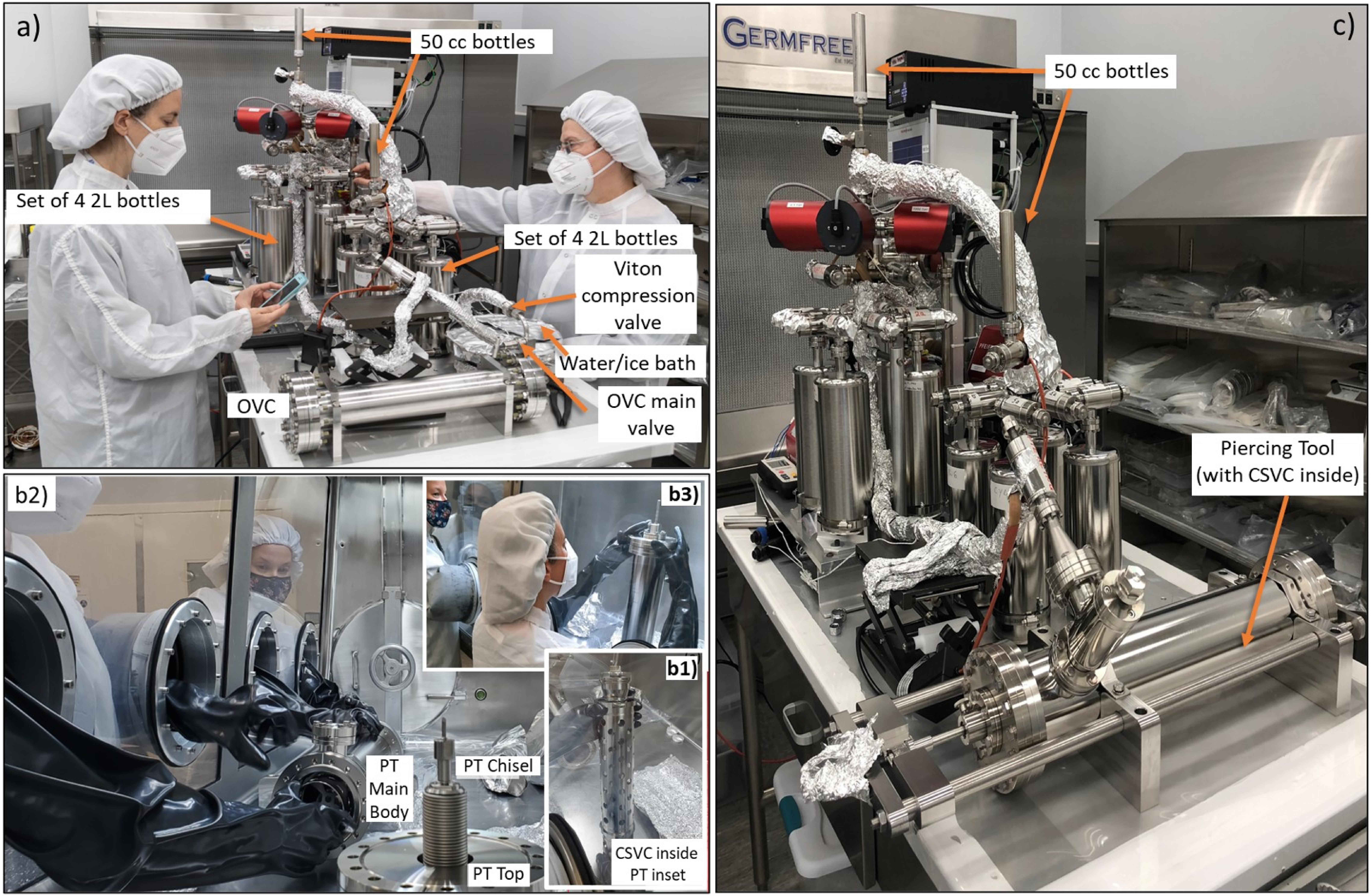

a)
50 cc bottles
Set of 4 2L bottles
Set of 4 2L bottles
Viton compression valve
Water/ice bath
OVC
OVC main valve
b2)
PT Main Body
PT Chisel
PT Top
b3)
b1)
CSVC inside PT inset
c)
GERMFREE
50 cc bottles
Piercing Tool (with CSVC inside)

Figure 6.

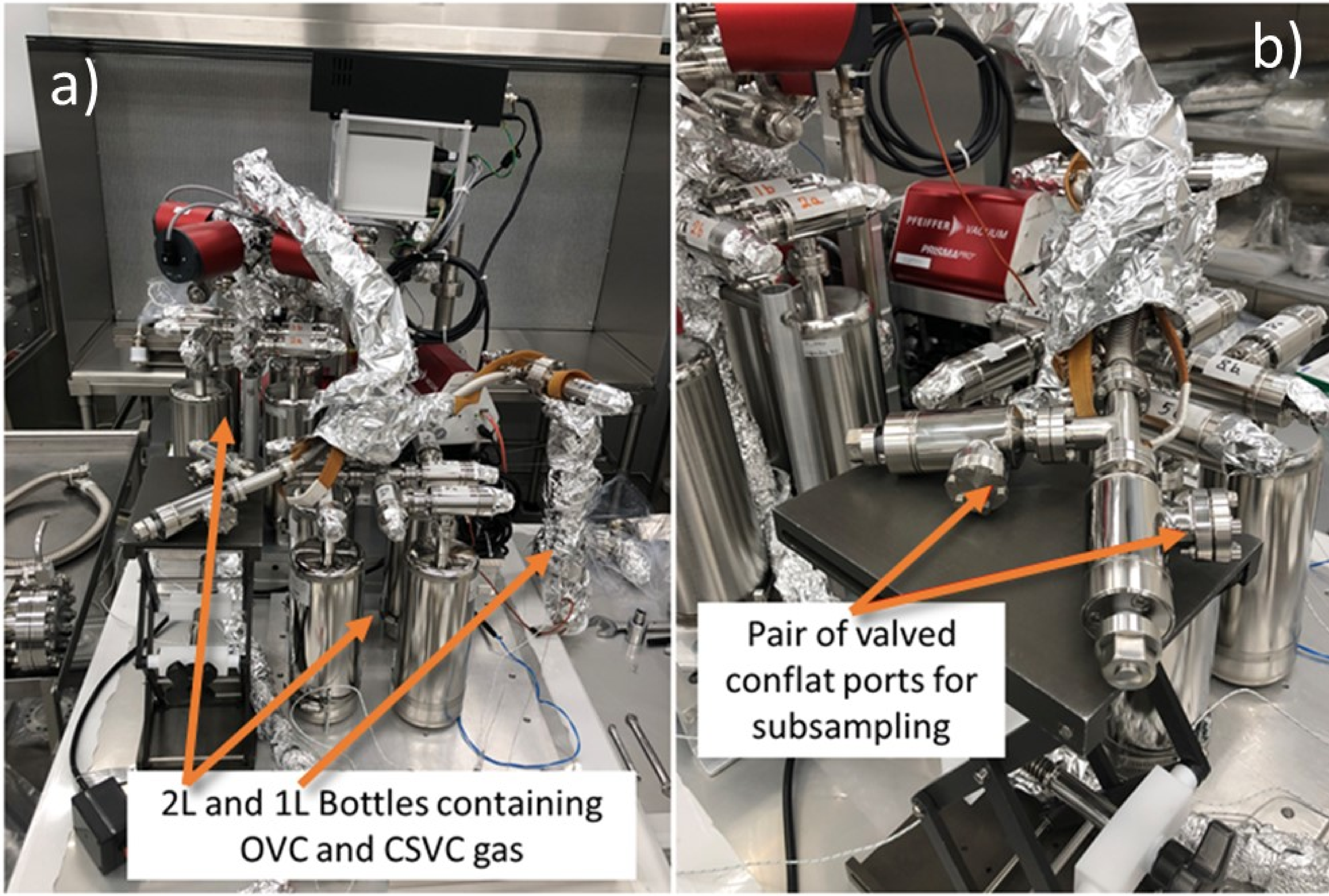
a)
2L and 1L Bottles containing
OVC and CSVC gas
b)
Pair of valved
conflat ports for
subsampling

Figure 7.

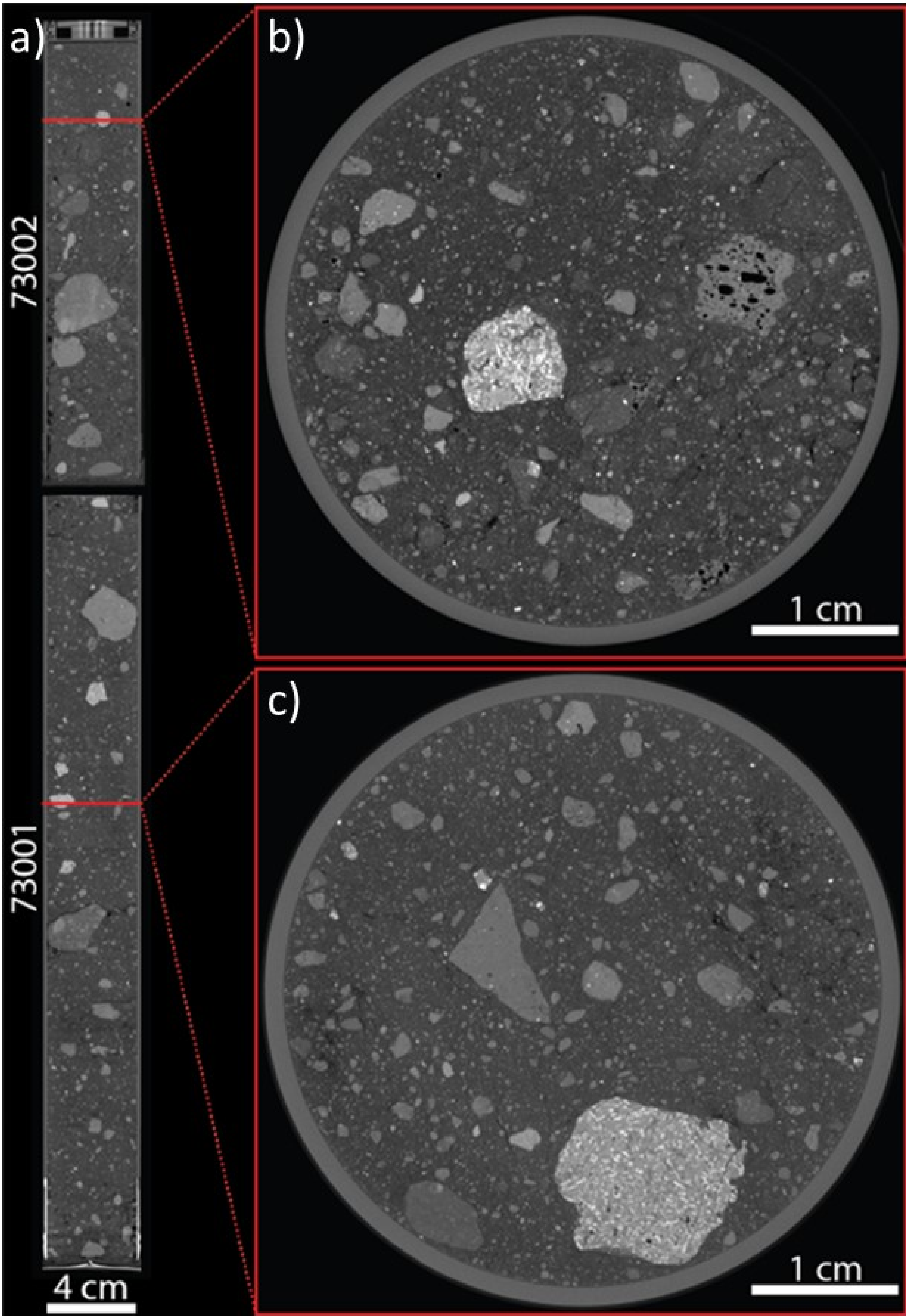
a)
73002
73001
4 cm
b)
1 cm
c)
1 cm

Figure 8.

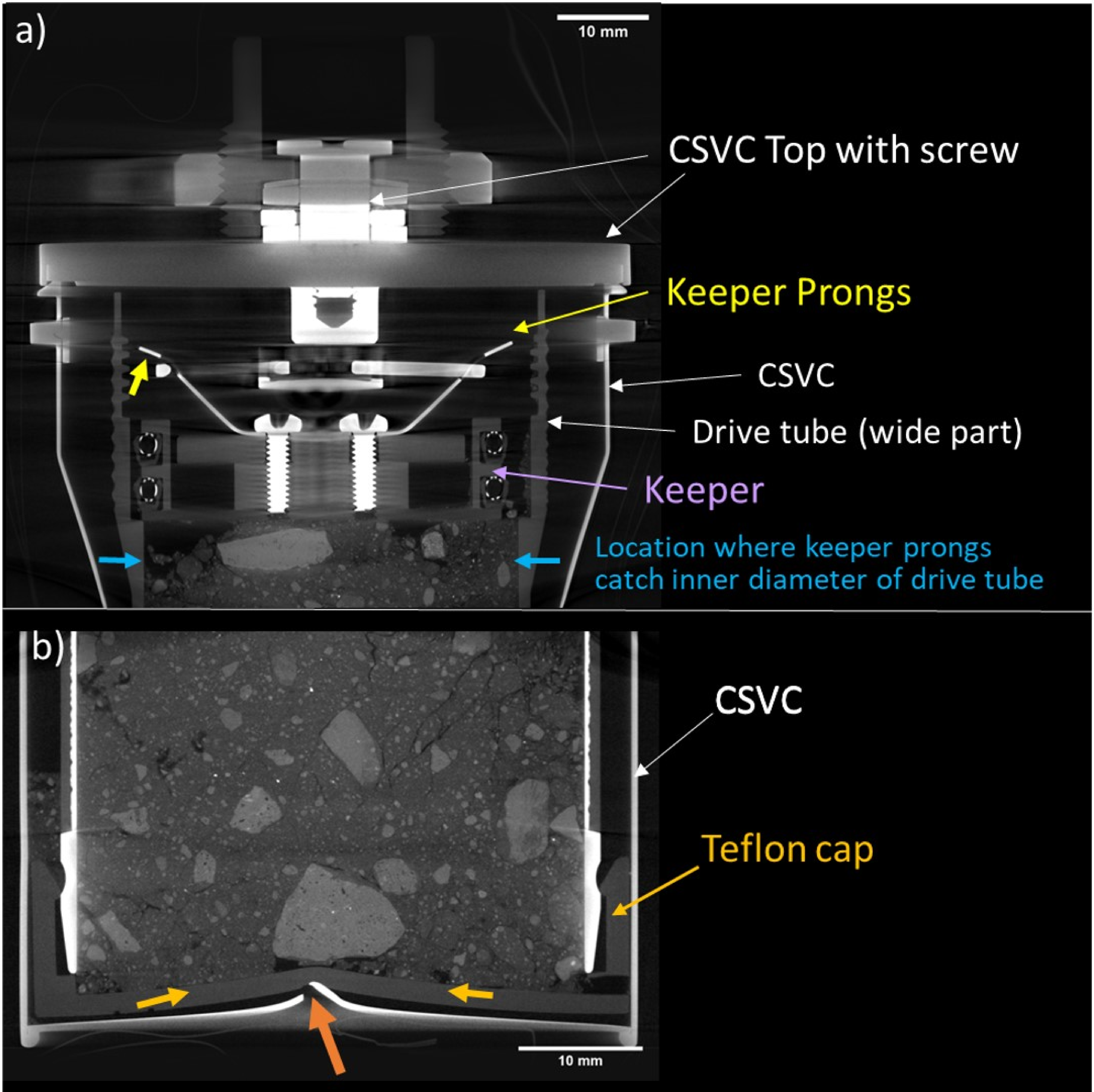
a)
10 mm
CSVC Top with screw
Keeper Prongs
CSVC
Drive tube (wide part)
Keeper
Location where keeper prongs
catch inner diameter of drive tube
b)
CSVC
Teflon cap
10 mm

Figure 9.

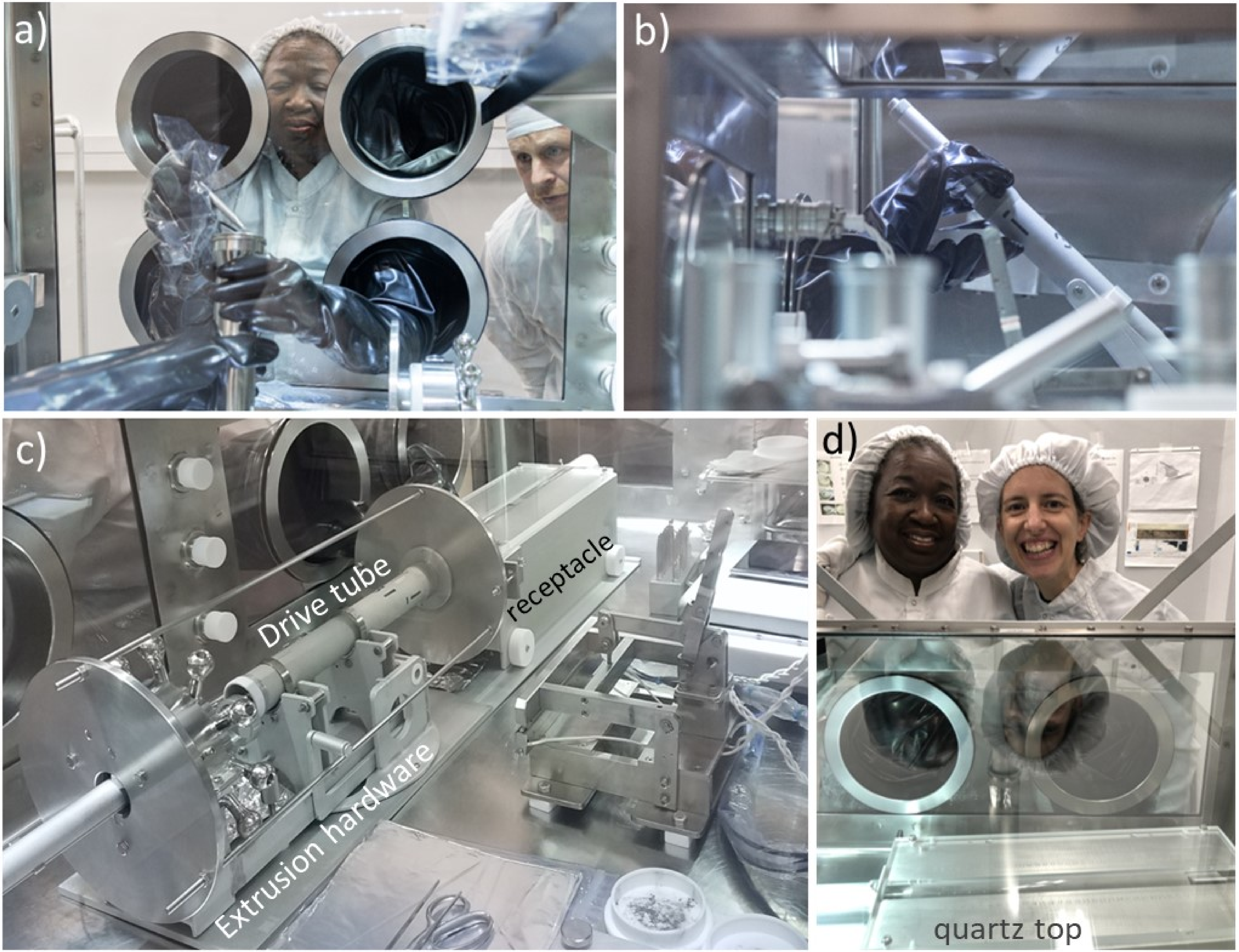
a)
b)
c)
Drive tube
receptacle
Extrusion hardware
d)
quartz top

Figure 10.


N
S
Bottom
(below surface)
Top (lunar surface)
Pass 1
Pass 2
Pass 3
TS
qtz top
1
2
3
4
5
a)
b)

Figure 11.

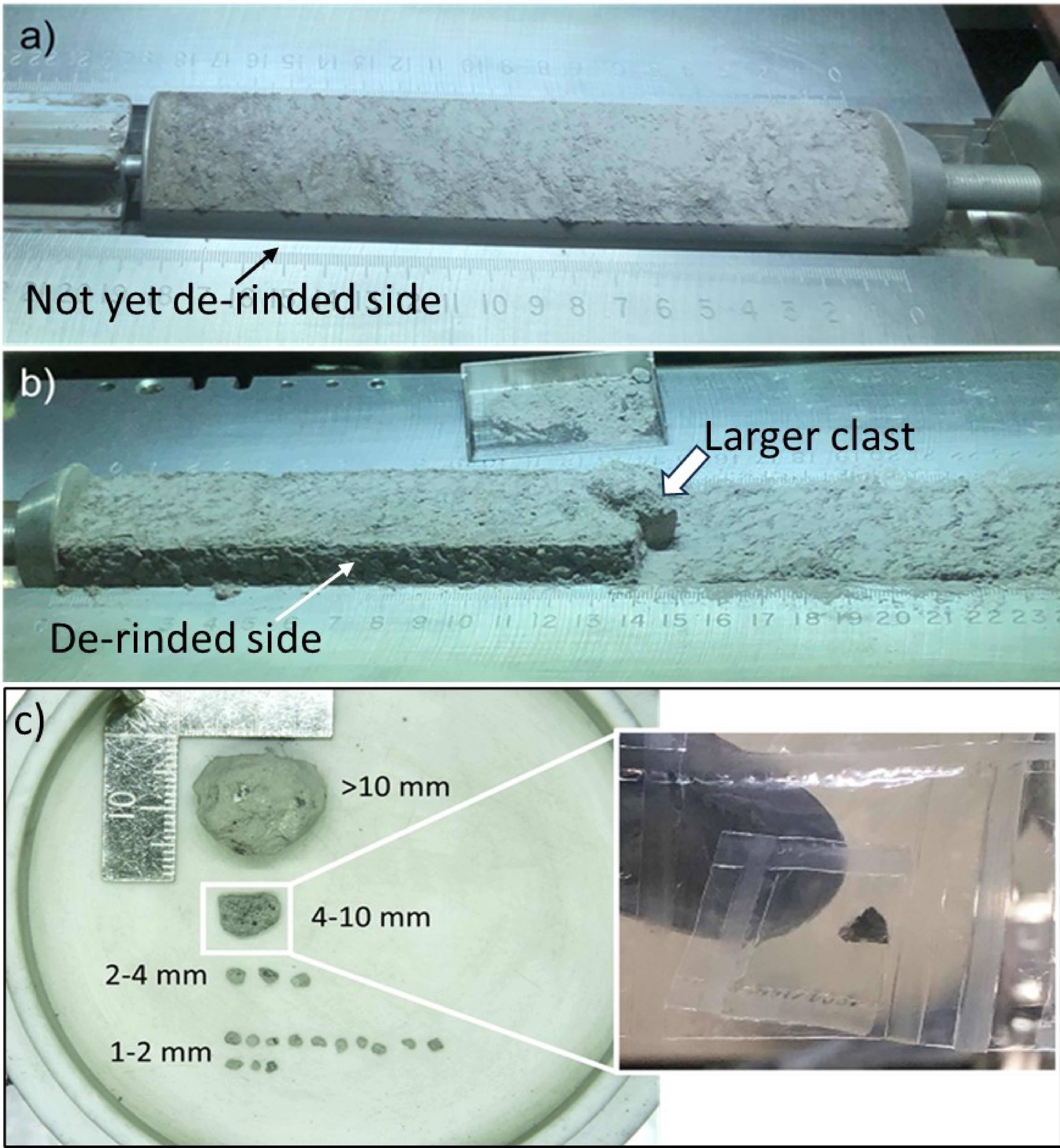

a)
Not yet de-rinded side
b)
Larger clast
De-rinded side
c)
>10 mm
4-10 mm
2-4 mm
1-2 mm

Figure 12.

a)

Interval information			Number of clasts					Mass (g)				
Interval #	*Depth beneath surface (cm):*	Total interval mass (g)	>10 mm	4-10 mm	2-4 mm	1-2 mm	Total # clasts	>10 mm	4-10 mm	2-4 mm	1-2 mm	<1 mm fines
1	*0.0 - 0.5*	2.001	0	0	7	7	14	0.000	0.000	0.062	0.023	1.916
2	*0.5 - 1.0*	2.273	0	1	11	8	20	0.000	0.050	0.080	0.017	2.126
3	*1.0 - 1.5*	2.963	0	3	11	20	34	0.000	0.193	0.121	0.066	2.583
4	*1.5 - 2.0*	2.943	0	1	13	36	50	0.000	0.100	0.080	0.131	2.632
5	*2.0 - 2.5*	2.754	0	5	13	19	37	0.000	0.244	0.094	0.054	2.362
6	*2.5 - 3.0*	3.012	0	2	11	29	42	0.000	0.148	0.133	0.092	2.639

Labelled >10 mm and 4-10 mm in					
Clast	Number (73002,xxx)	Size fraction (mm)	Individual mass (g)	CT scanned (Y, N)	CT mov made (
B	,1009	4-10	0.128	Y	x
B	,1017	4-10	0.098	Y	x
B	,1021	4-10	0.025	Y	x

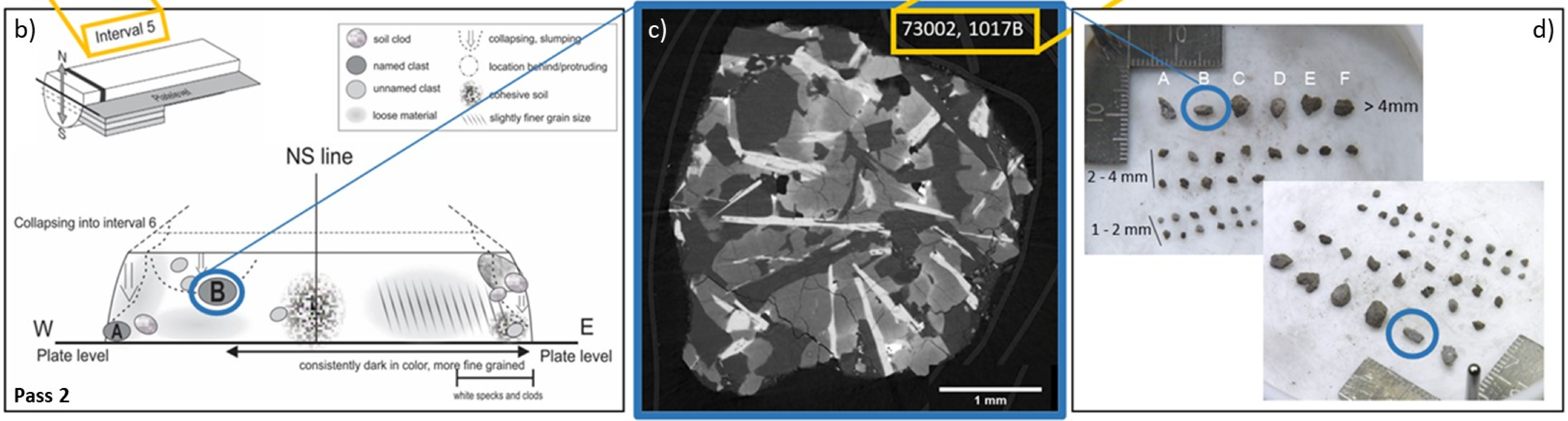

Figure 13.

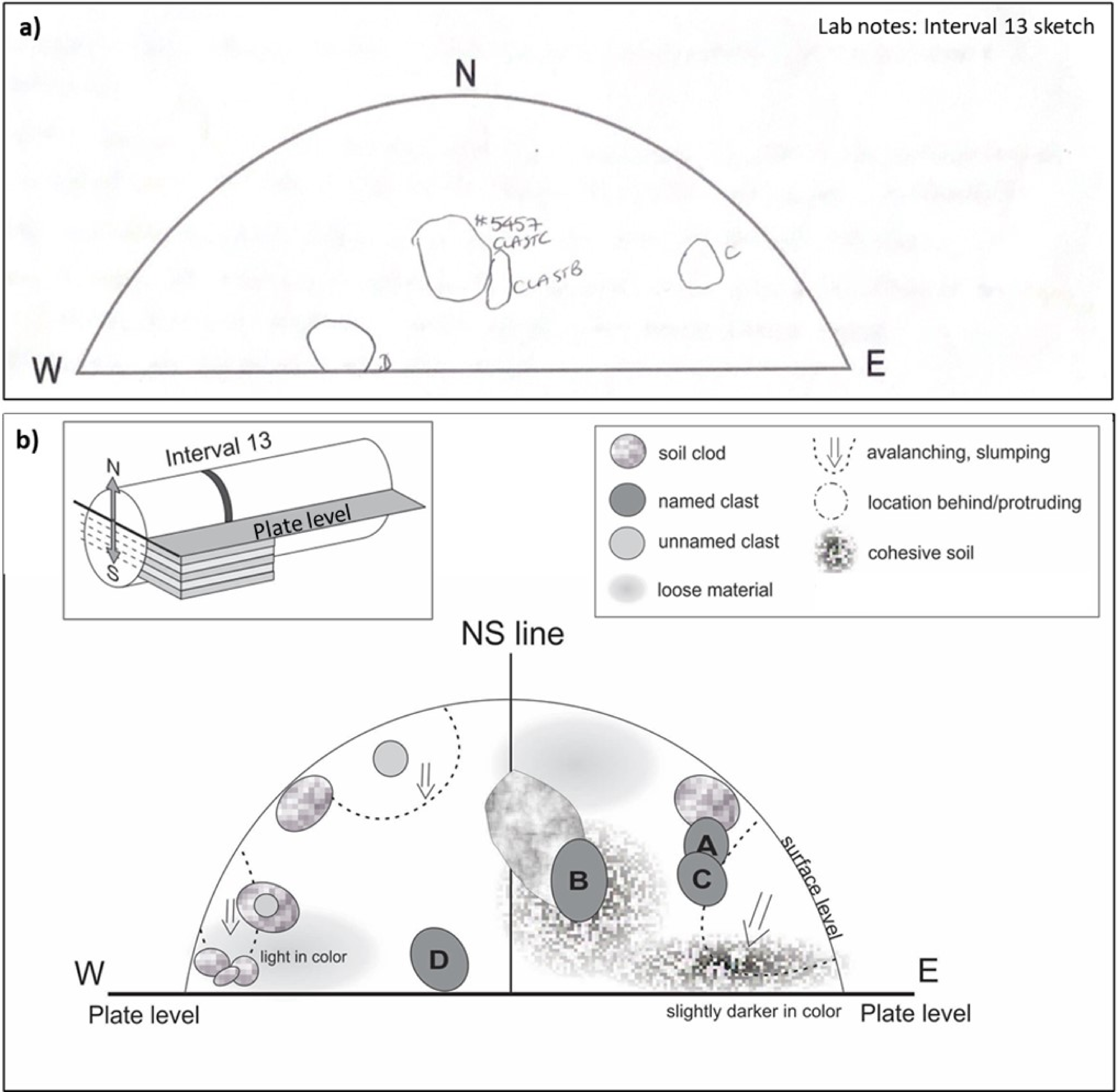

a)
Lab notes: Interval 13 sketch
N
W
E
#5457
CLAST C
CLAST B
C
D
b)
Interval 13
N
S
Plate level
soil clod
named clast
unnamed clast
loose material
avalanching, slumping
location behind/protruding
cohesive soil
NS line
A
B
C
D
surface level
light in color
slightly darker in color
W
E
Plate level
Plate level

Figure 14.

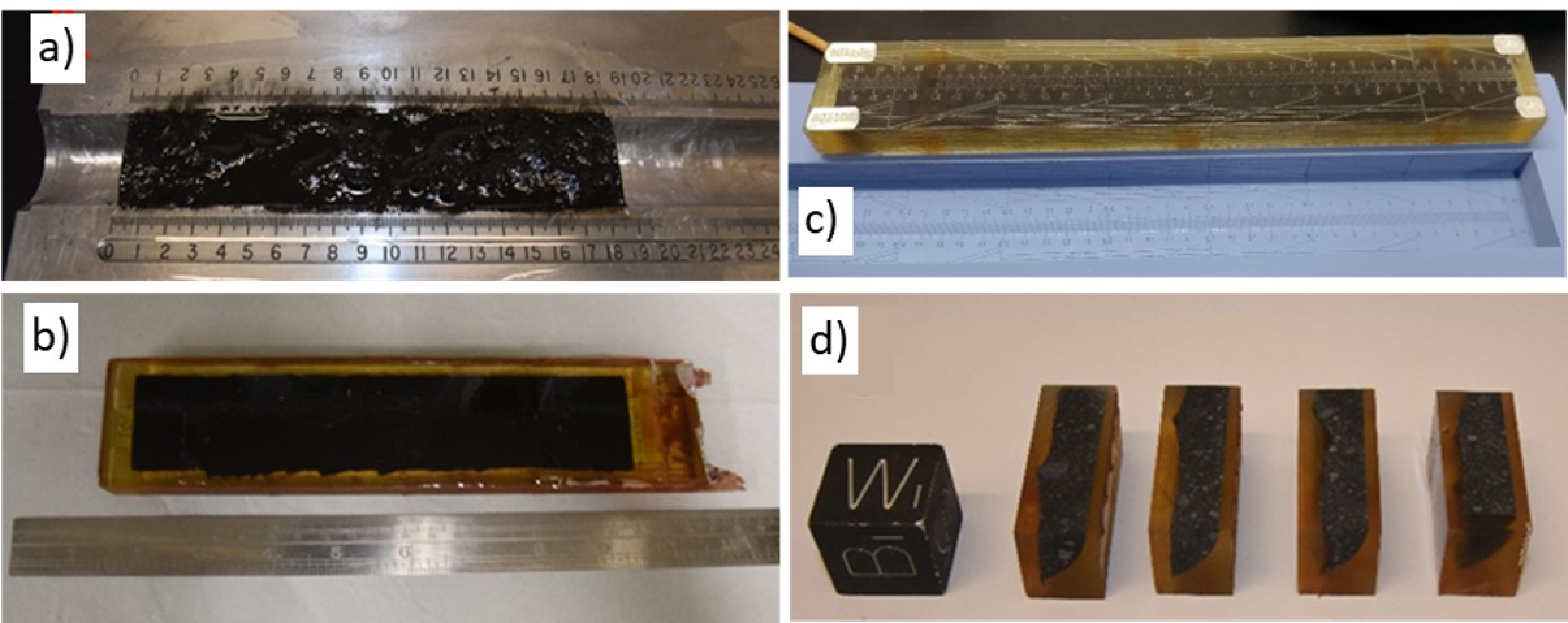
a)
b)
c)
d)

Figure 15.

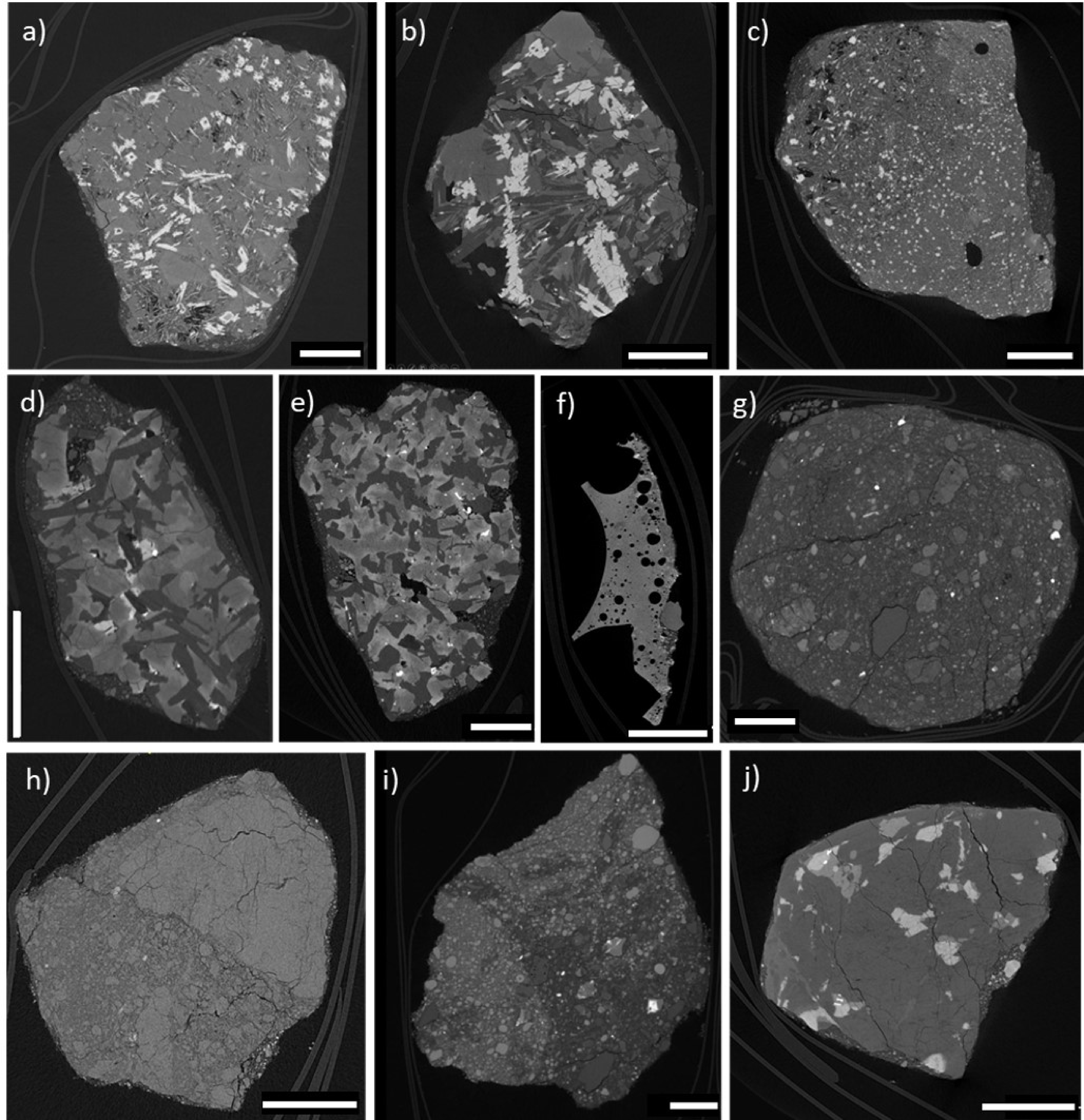
a)
b)
c)
d)
e)
f)
g)
h)
i)
j)

Figure 16.

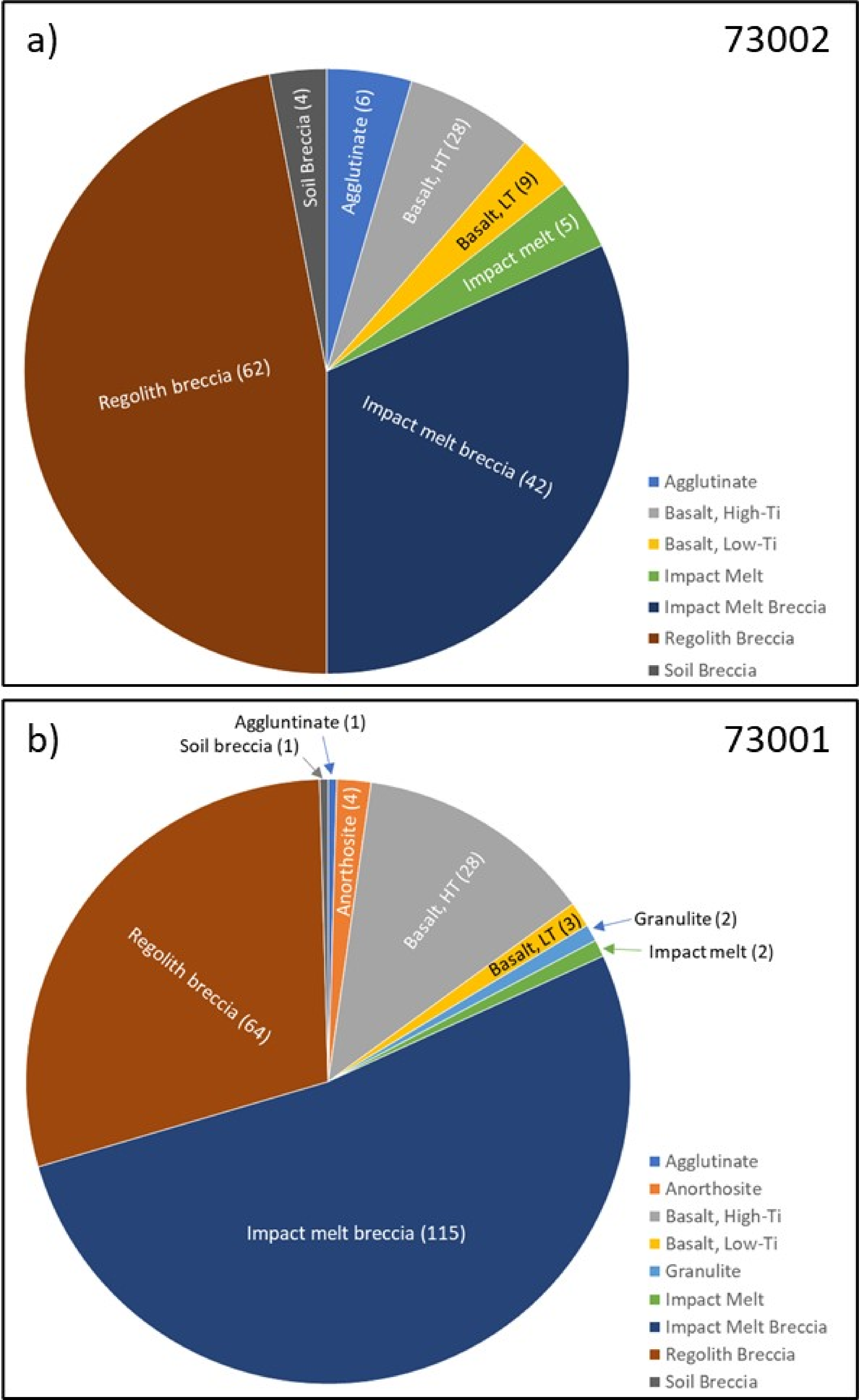
a)
73002
Soil Breccia (4)
Agglutinate (6)
Basalt, HT (28)
Basalt, LT (9)
Impact melt (5)
Regolith breccia (62)
Impact melt breccia (42)
Agglutinate
Basalt, High-Ti
Basalt, Low-Ti
Impact Melt
Impact Melt Breccia
Regolith Breccia
Soil Breccia
b)
73001
Aggluntinate (1)
Soil breccia (1)
Anorthosite (4)
Basalt, HT (28)
Granulite (2)
Basalt, LT (3)
Impact melt (2)
Regolith breccia (64)
Impact melt breccia (115)
Agglutinate
Anorthosite
Basalt, High-Ti
Basalt, Low-Ti
Granulite
Impact Melt
Impact Melt Breccia
Regolith Breccia
Soil Breccia

Figure 17.

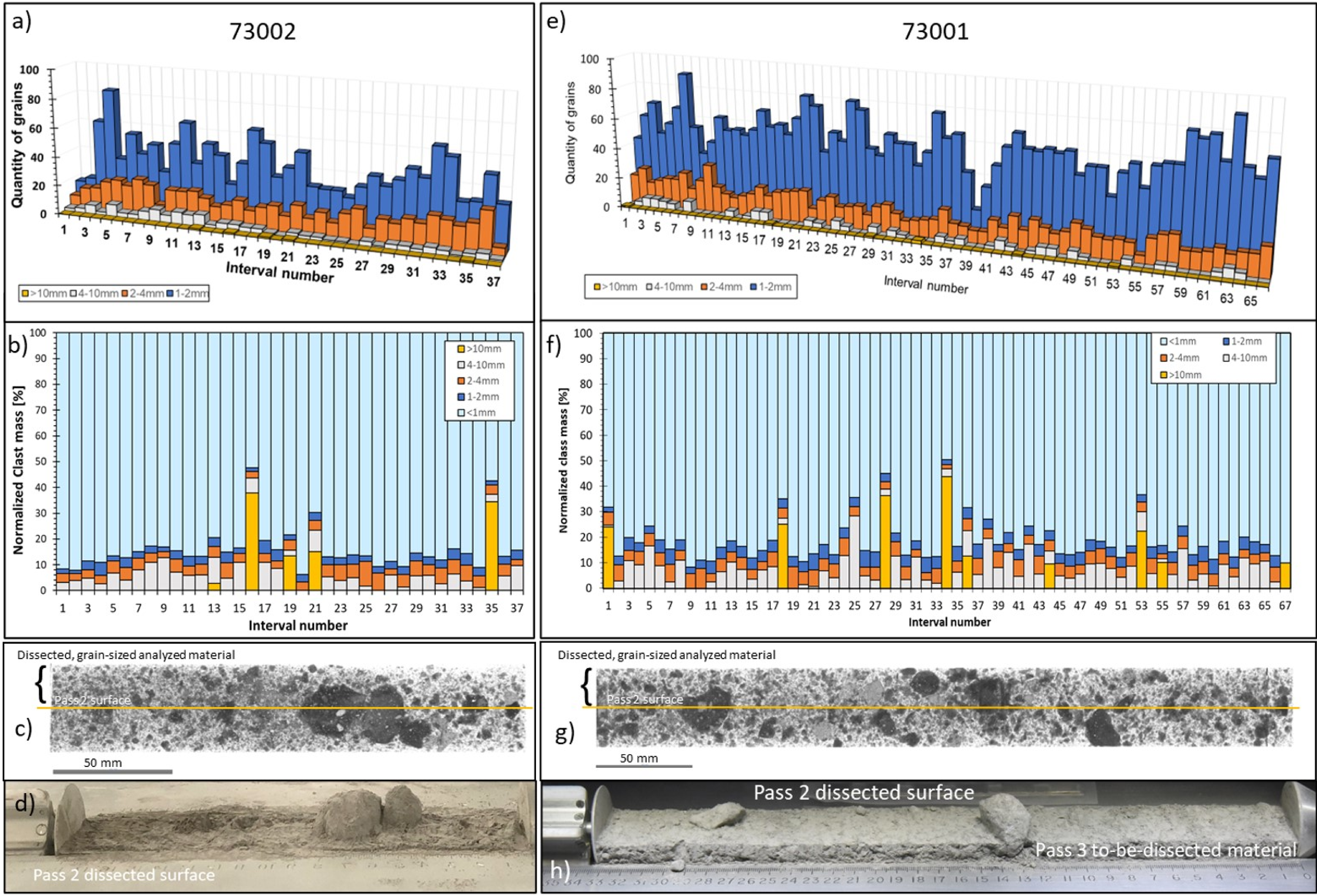

a)
73002
Quantity of grains
Interval number
>10mm 4-10mm 2-4mm 1-2mm
e)
73001
Quantity of grains
Interval number
>10mm 4-10mm 2-4mm 1-2mm
b)
Normalized Clast mass [%]
Interval number
>10mm
4-10mm
2-4mm
1-2mm
<1mm
f)
Normalized class mass [%]
Interval number
<1mm
1-2mm
2-4mm
4-10mm
>10mm
c)
Dissected, grain-sized analyzed material
Pass 2 surface
50 mm
g)
Dissected, grain-sized analyzed material
Pass 2 surface
50 mm
d)
Pass 2 dissected surface
h)
Pass 2 dissected surface
Pass 3 to-be-dissected material

Figure 18.

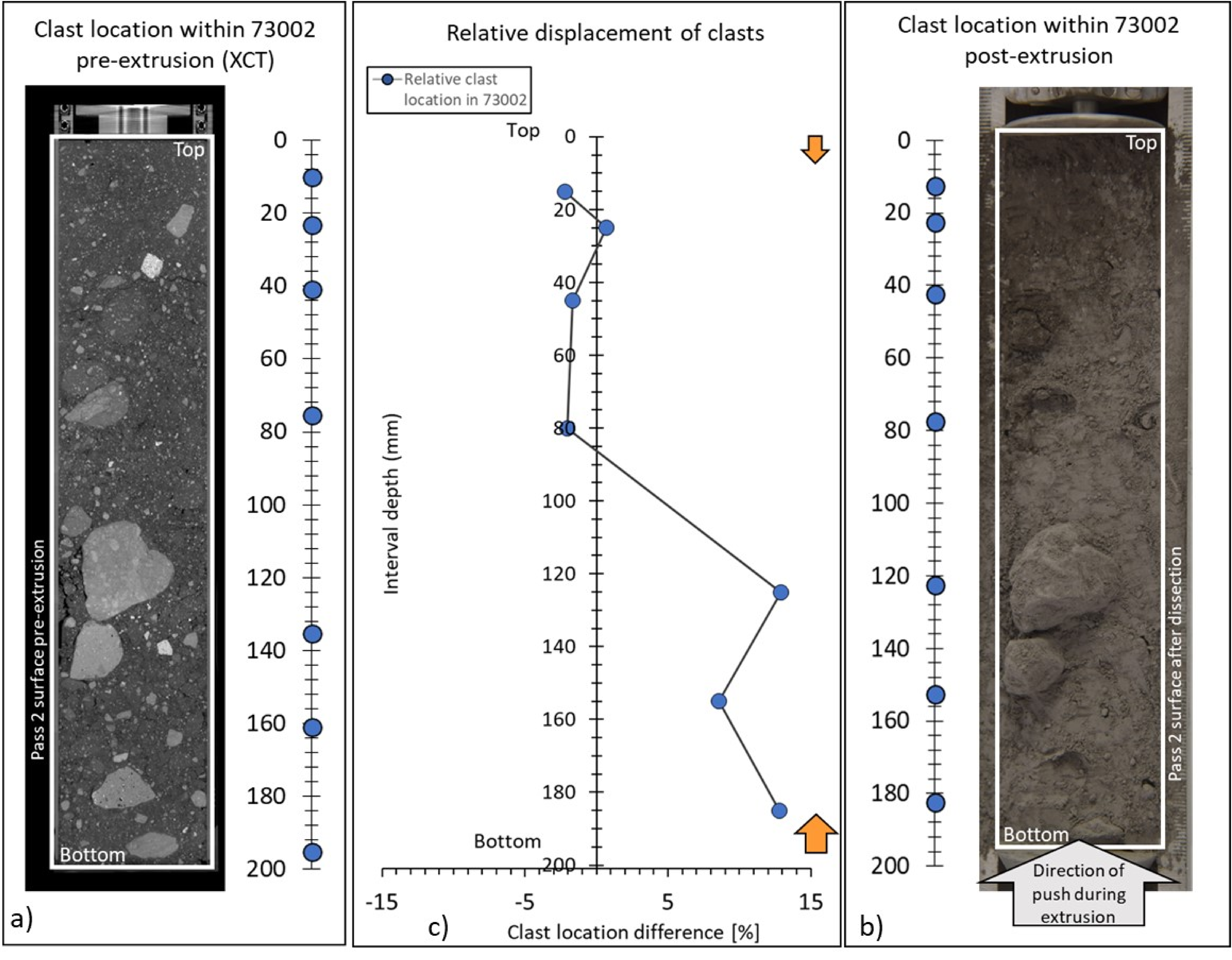

Clast location within 73002 pre-extrusion (XCT)
Top
Bottom
Pass 2 surface pre-extrusion
0
20
40
60
80
100
120
140
160
180
200
a)
Relative displacement of clasts
Relative clast location in 73002
Top
Bottom
Interval depth (mm)
-15
-5
5
15
c)
Clast location difference [%]
Clast location within 73002 post-extrusion
Pass 2 surface after dissection
Direction of push during extrusion
b)

Figure 19.

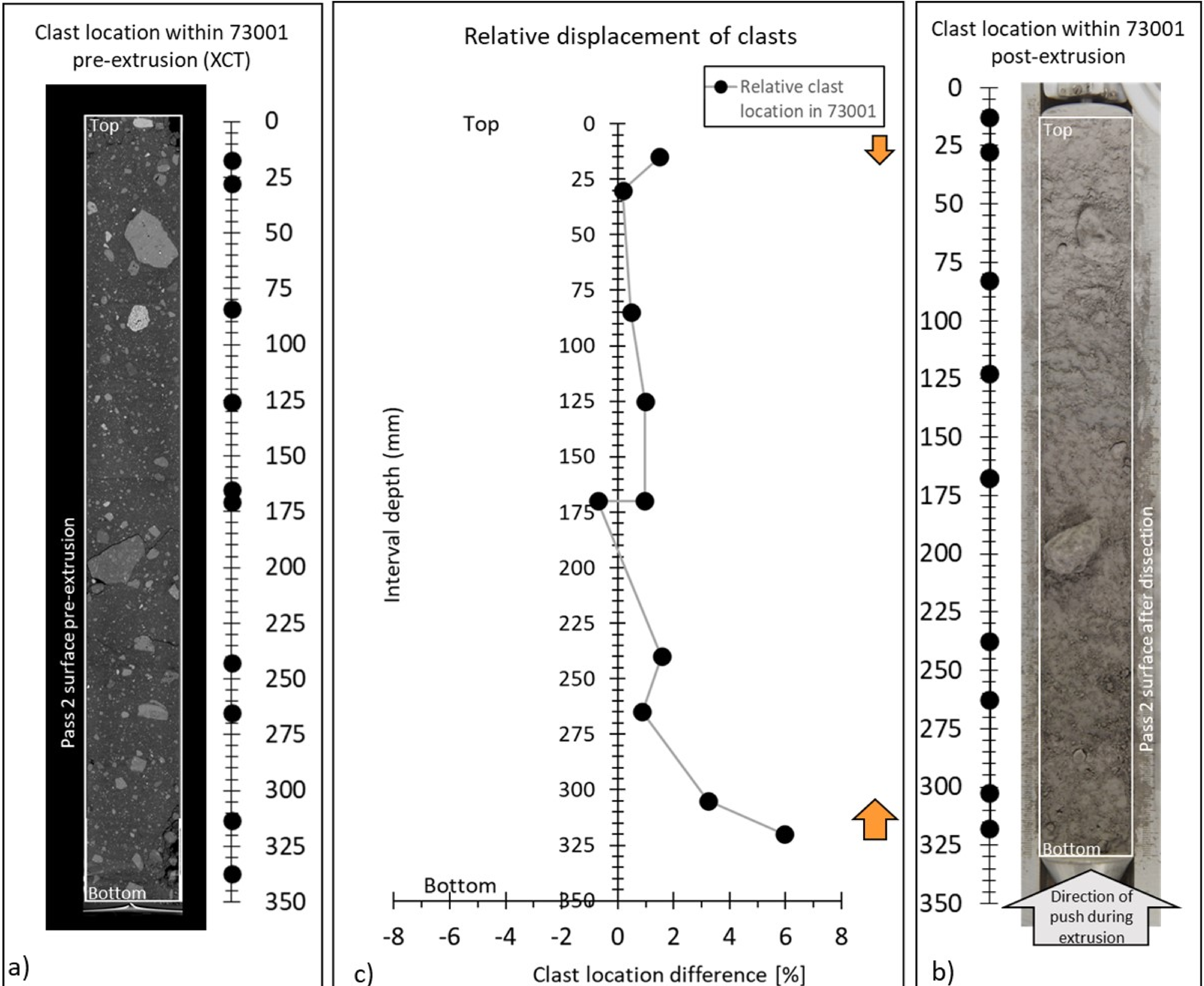

Clast location within 73001 pre-extrusion (XCT)
Top
Bottom
Pass 2 surface pre-extrusion
0
25
50
75
100
125
150
175
200
225
250
275
300
325
350
a)
Relative displacement of clasts
Relative clast location in 73001
Top
Bottom
Interval depth (mm)
-8
-6
-4
-2
0
2
4
6
8
Clast location difference [%]
c)
Clast location within 73001 post-extrusion
Pass 2 surface after dissection
Direction of push during extrusion
b)

Table 1: List of Gas Samples Taken from ANGSA Sample 73001							
Sample Number		**Container number**	**Container Volume**	**Container Press (Torr)**	**Type of Gas in the Container**	**Equilibration time**	**Notes**
Generic	**Specific**						
73001	,5001	4	~1.9 liter	~5 x 10-6	System Blank	15 minutes	
73001	,5002	3	~1.9 liter	27	OVC, 1st extraction	15 minutes	
73001	,5003	2	~1.9 liter	7	OVC, 2nd extraction	15 minutes	
73001	,5004	1	~1.9 liter	~0.2	CSVC, Leak Gas 1	15 minutes	Accumulated in the piercing tool for ~24 hours prior to extraction
73001	,5005	8	~1.9 liter	~0.2	CSVC, Leak Gas 2	15 minutes	Accumulated in the piercing tool for ~24 hours prior to extraction
73001	,5006	6	~1.9 liter	4.6	CSVC, 1st extraction	15 minutes	
73001	,5007	7	~1.9 liter	4.6	CSVC, 1st extraction	15 minutes	
73001	,5008	5	~1.9 liter	3.2	CSVC, 2nd extraction	10.75 days	
73001	,5009	9	~1 liter	5 x 10-4	CSVC, 3rd extraction	15 minutes	Piercing Tool/CSVC was pumped down to 2 x 10-7 Torr, and then gas accumulated in sealed piercing tool for 6 days prior to extraction
73001	,5010	10	50 cc	28	OVC, 1st extraction	15 minutes	Consumed for PE
73001	,5011	11	50 cc	4.6	CSVC, 1st extraction	15 minutes	Consumed for PE

Table 2: Lithologic Classification of >4 mm particles by XCT				
73001				
Lithology	**# of particles**	**% of particles**	**Mass of particles (g)**	**% of mass**
Agglutinate	1	0.5%	0.112	0.1%
Anorthosite	4	1.8%	0.200	0.2%
Basalt, High-Ti	28	12.7%	6.736	7.6%
Basalt, Low-Ti	3	1.4%	0.216	0.2%
Granulite	2	0.9%	0.194	0.2%
Impact Melt	2	0.9%	1.528	1.7%
Impact Melt Breccia	115	52.3%	50.745	56.9%
Regolith Breccia	64	29.1%	29.360	32.9%
Soil Breccia	1	0.5%	0.086	0.1%
73002				
Lithology	**# of particles**	**% of particles**	**Mass of particles (g)**	**% of mass**
Agglutinate	6	4.5%	0.143	0.3%
Anorthosite	0	0.0%	0.000	0.0%
Basalt, High-Ti	9	6.8%	1.639	2.9%
Basalt, Low-Ti	4	3.0%	0.291	0.5%
Granulite	0	0.0%	0.000	0.0%
Impact Melt	5	3.8%	0.247	0.4%
Impact Melt Breccia	42	31.8%	18.732	33.1%
Regolith Breccia	62	47.0%	35.118	62.1%
Soil Breccia	4	3.0%	0.361	0.6%